Expert Systems With Applications 186 (2021) 115356

Contents lists available at ScienceDirect

Expert Systems With Applications

journal homepage: www.elsevier.com/locate/eswa

Bead geometry modeling on uneven base metal surface by fuzzy systems for multi-pass welding

Csongor Márk Horváth [a,b,*], János Botzheim [a], Trygve Thomessen [b], Péter Korondi [a]

[a] Department of Mechatronics, Optics and Mechanical Engineering Informatics, Faculty of Mechanical Engineering, Budapest University of Technology and Economics, 1111 Budapest, Műegyetem rkp. 3., Hungary
[b] PPM Robotics AS, Leirfossvegen 27, 7038 Trondheim, Norway

ARTICLE INFO

Keywords:
Multi-pass Welding
Weld Bead Profile Modeling
Bacterial Memetic Algorithm
Fuzzy Systems
Machine Learning

ABSTRACT

This paper presents a modeling method of weld bead profiles deposited on uneven base metal surfaces and its application in multi-pass welding. The robotized multi-pass tungsten inert gas welding requires precise positioning of the weld beads to avoid welding defects and achieve the desirable welding join since the weld bead shapes depend on the surface of the previously deposited beads. The proposed model consists of fuzzy systems to estimate the coefficients of the profile function. The characteristic points of the trapezoidal membership functions in the rule bases are tuned by the Bacterial Memetic Algorithm during supervised training. The fuzzy systems are structured as multiple-input-single-output systems, where the inputs are the welding process variables and the coefficients of the shape functions of the segments underlying the modeled bead; the outputs are the coefficients of the bead shape function. Each segment surface is approximated by a second-order polynomial function defined in the weld bead's local coordinate system. The model is developed from empirical data collected from single and multi-pass welding. The performance of the proposed model is compared with a multiple linear regression model. During the experimental validation, first, the individual beads are evaluated by comparing the estimated coefficients of the profile function and other bead characteristics (bead area, width, contact angles, and position of the toe points) with the measurements, and the estimations of a multiple linear regression model. Second, the sequential placement of the weld beads is evaluated while filling a straight V-groove by comparing the estimated bead characteristics with the measurements and calculating the accumulated error of the filled groove cross-section. The results show that the proposed model provides a good estimation of the bead shapes during deposition on uneven base metal surfaces and outperforms the regression model with low error in both validation cases. Furthermore, it is experimentally validated that the derived bead characteristics provide a suitable measure to identify locations sensitive to welding defects.

1. Introduction

Automated welding systems are developed and used mostly for mass production in the automotive industry. Although, robotization of small series and one-of-a-kind production gained more attention in the last years, primarily used by small and medium-sized enterprises. A wide variety of robotic welding systems provide quality and efficient solutions for the general welding industry. Still, skilled employees cannot be replaced yet in the welding of joints in complex structures due to the robots' long commissioning time and tedious teaching procedure.

Manufacturing one-of-a-kind products, such as the heavy-duty Francis hydro-power turbines (Horvath, Thomessen, & Korondi, 2017), is typically a task with low repeatability due to the workpiece's complex geometry. Off-line robot programming methods are applied to overtake the difficulties (Madsen, Bro Soerensen, Larsen, Overgaard, & Jacobsen, 2002; Pires, Loureiro, & Bolmsjö, 2006; Tarn, Chen, & Fang, 2011) by creating collision-free motion in the access restricted zones (Lee et al., 2011; Fang, Ong, & Nee, 2016), and providing a graphical user interface for control during the inter-task trajectories and welding paths (Fang, Ong, & Nee, 2012; Liu et al., 2015; Liu, Zhang, & Zhang, 2015).

Further challenges are uprising to handle the significant changes in

* Corresponding author at: Department of Mechatronics, Optics and Mechanical Engineering Informatics, Faculty of Mechanical Engineering, Budapest University of Technology and Economics, 1111 Budapest, Hungary.
E-mail addresses: hcsongorm@mogi.bme.hu (C.M. Horváth), dr.janos.botzheim@ieee.org (J. Botzheim), trygve.thomessen@ppm.no (T. Thomessen), korondi@mogi.bme.hu (P. Korondi).

https://doi.org/10.1016/j.eswa.2021.115356
Received 13 July 2020; Received in revised form 20 January 2021; Accepted 4 June 2021
Available online 21 July 2021

the base metal thickness, thus the groove's depth and the variety in the groove opening angle (Yan, Fang, Ong, & Nee, 2017). The groove's complexity is similar to the joints in the shipbuilding and offshore industry, where the thick-plate welding accounts for approximately 70 percent of the total welding jobs. This results a low productivity rate by conventional methods such as manual or semi-automatic welding. The large dimension joints of thick plates or pipes mean deep and voluminous grooves and cannot be filled with single-pass welding; therefore, multi-pass welding becomes necessary.

Defining the connection between the shapes of the weld beads and welding process variables is necessary to control the deposition successfully. It has been intensively studied regarding multi-pass welding (Cao, Zhu, Liang, & Wang, 2011; Fang, Ong, & Nee, 2017; Horváth & Korondi, 2018; Somlo & Sziebig, 2019), and similarly in additive manufacturing (DebRoy et al., 2018; Yuan et al., 2020; Wang et al., 2020). Traditionally, the main parameters of controlling the bead shape are the width, the height, the area, and the describing function. Area-based simplification of the beads' shapes as parallelograms and trapezoids are used by Madsen et al. (2002),Yang, Ye, Chen, Zhong, and Chen (2014) and Zhang, Lu, Cai, and Chen (2011) to generate the bead pattern in multi-pass welding. However, the authors have admitted that a supportive sensory system might be required for regular adjustments due to the implementation's inaccuracy.

In additive manufacturing using arc welding, Cao et al. (2011) conducted research on a finer bead shape estimation using regular curves: sine, cosine, arc, parabola, Gaussian, and logistic functions. The functions' coefficients contained the bead width and height. To achieve a stable layering, precise control of the height is required, directly related to the bead shape function and the distance between the adjacent bead's centerlines. Cao et al. (2011) suggested the sine and the parabola function as the best candidates to describe the bead shape. Similarly, the parabola was found as the best fitting curve by Ding, Pan, Cuiuri, and Li (2015), Suryakumar et al. (2011), and Xiong, Zhang, Gao, and Wu (2013). However, the latter author added that the wire feed rate ratio to the welding speed plays an important role. The parabola model in metal inert gas (MIG) welding can be used if this ratio is under 12.5; above that value, the arc model is suitable.

A parabola can describe the shape of the weld beads, and its parameters depend on the welding process variables and material properties, preferably described by a suitable model. The statistical and numerical approaches were developed since they required less computational power. Such models were reviewed by Benyounis and Olabi (2008) in general and presented for MIG and tungsten inert gas (TIG) welding by several researchers (Dutta & Pratihar, 2007; Palani & Murugan, 2007; Xiong, Zhang, Hu, & Wu, 2014; Schneider, Lisboa, Silva, & Lermen, 2017). Recently, computational intelligence and machine learning became dominant in the field (Pratihar, 2015; Feng, Chen, Wang, Chen, & Feng, 2020), providing base bead models for intelligent welding systems (Fan, Zhang, Shi, and Zhu, 2019).

Computational intelligence (CI) techniques, such as neural networks, fuzzy systems, and evolutionary algorithms, are widely used to solve complex and non-linear problems. Even more, several hybrid computing techniques were developed to compensate for their limitations (Gowtham, Vasudevan, Maduraimuthu, & Jayakumar, 2011). In welding, most computational intelligence techniques can be used as demonstrated for neural network-based cases (Kim, Son, Park, Lee, & Prasad, 2002; Mishra et al., 2007; Dutta & Pratihar, 2007; Xiong et al., 2014; Ding et al., 2016) or for fuzzy systems (Hancheng, Bocai, Shangzheng, & Fagen, 2002; Xue et al., 2005; Narang, Singh, Mahapatra, & Jha, 2011; Subashini & Vasudevan, 2012). They provide sufficient prediction for the bead shape parameters like width, height, or area without considering the bead describing function. However, the experimental models' performance is highly influenced by the experimental data sets' quality and, consequently, narrowed to the application's specific validity range. Correspondingly, several settings should keep constant such as the compound of base material and the filler wire, the welding method, and most environmental properties. A further benefit of a model could be to detect welding defects (Liao, 2003; Alfaro & Franco, 2010; Meng, Qin, & Zou, 2017).

CI techniques' important common feature is that they usually provide approximate, acceptably suboptimal solutions while keeping the computational complexity at a tractable (usually low degree polynomial) level. Neural networks and fuzzy systems (FS) are universal approximators (Wang, 1992; Kurková, 1992), and they can be transformed into each other. As Koczy (1996) showed, the Takagi–Sugeno-Kang (TSK) FS is asymptotically equivalent to the Mamdani FS model and can be transformed into each other. Therefore, any architecture choice can be justified (Jang & Sun, 1993; Koczy, 1996; Koczy, Tikk, & Gedeon, 2000).

One of the main advantages of choosing fuzzy systems is the inference base, which provides human-like reasoning due to the fuzzy system's rule-based approach and non-linear mapping of inputs. They offer an easily interpretable method, where the arguments leading to the conclusion can be assessed from the rule base (Kesse, Buah, Handroos, & Ayetor, 2020). The main challenge is to find a sufficient number of rules and the optimal definition of the membership functions. The tuning of the membership functions' parameters can be done by training (Botzheim, Cabrita, Koczy, & Ruano, 2004), allowing the fuzzy systems to learn from the data. In many different fields, evolutionary algorithms are applied to design fuzzy systems (Cordón, 2001; Botzheim, Cabrita, Kóczy, & Ruano, 2009; Fernandez, Herrera, Cordon, Jose del Jesus, & Marcelloni, 2019). With the ability to solve and quasi-optimize problems with non-linear and discontinuous characteristics, several evolutionary optimization algorithms were developed (Bartz-Beielstein, Branke, Mehnen, & Mersmann, 2014; Doerr & Neumann, 2020; Nawa & Furuhashi, 1999). The main disadvantage of the classical evolutionary algorithms is the low convergence speed in the optimization process. Combining them with gradient-based local search methods can utilize the advantages of both methods leading to the memetic algorithms (Moscato, 1989).

Bacterial Memetic Algorithm (BMA) (Botzheim et al., 2009) is a memetic algorithm in which the bacterial evolutionary algorithm is used instead of the classical genetic algorithm, and the Levenberg–Marquardt (LM) method (Levenberg, 1944; Marquardt, 1963) is applied as a local search. The competitive performance of BMA is shown in several fields, for example, in optimization (Botzheim, Toda, & Kubota, 2012), supervised machine learning (Balázs, Botzheim, & Kóczy, 2010). Furthermore, BMA is applied in several combinatorial optimization problems (Botzheim et al., 2012; Zhou, Fang, Botzheim, Kubota, & Liu, 2016), in supervised machine learning tasks such as fuzzy rule base extraction (Botzheim et al., 2009) and training fuzzy neural networks (Botzheim & Földesi, 2014), and in single pass welding (Horváth, Botzheim, Thomessen, & Korondi, 2020), still its application in multi-pass welding is not explored.

The previously listed studies provided a geometrical description of single weld beads. The interaction between the deposited beads was also studied, and models developed as described by Cao et al. (2011) and Joshi, Hildebrand, Aloraier, and Rabczuk (2013), Xiong et al. (2013). The main principle of their models is that the adjacent beads overlap each other. At an ideal center distance, the overlapping area is equal to the valley area found at the top of the bead between the highest points. Different models, such as the Bead Overlapping Model (BOM) (Cao et al., 2011) and Tangent Overlapping Model, (Ding et al., 2015) provided a different solution for the optimal center-line distance value.

However, Ding et al. (2015) observed that it is impossible to achieve an ideally flat top surface between adjacent beads, which served as the primary motivation to Li, Sun, Han, Zhang, and Horváth (2018), who recently examined the overlapping models and introduced the spreading effect what the result of physical phenomena during the solidification process of the melted metal. The method reduces the surface unevenness by reducing the center distance between the first two deposited beads with a d_0 measured value and keeping the rest of the offset suggested by

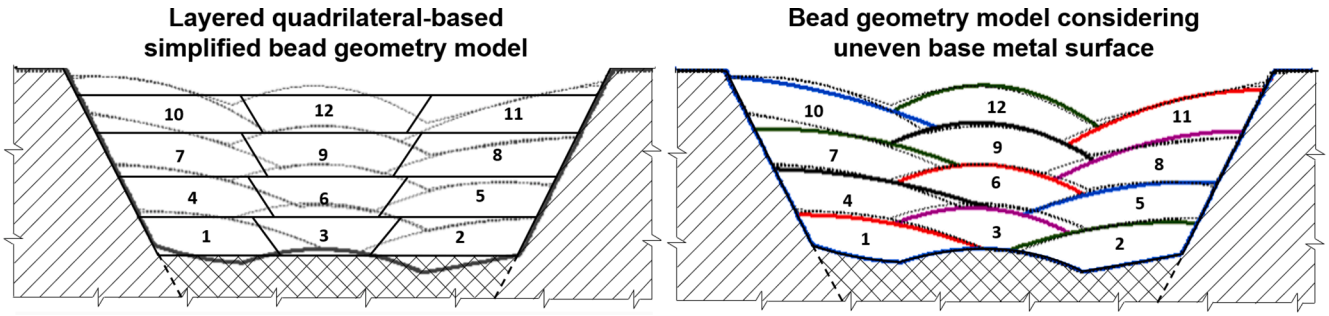

Fig. 1. Traditional weld bead representation compared to the proposed method. (Left) The weld bead shapes are simplified into quadrilaterals and organized into layers. (Right) The weld bead shapes are described with a polynomial function and placed freely on the uneven base metal surface.

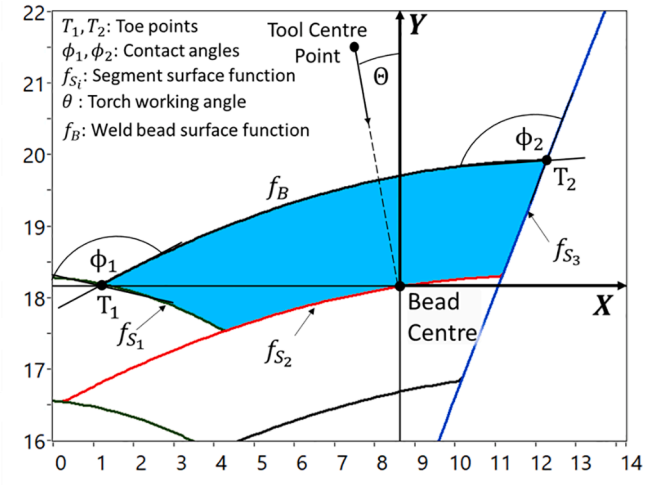

Fig. 2. Weld bead and its characteristics in a groove, deposited during multi-pass welding. The bead local coordinate system (LCS) is defined at the bead center.

the BOM. The d_0 is defined experimentally and refers to the average distance between the right half of the assumed and the actual profile cross-section profile of the second bead at a given vertical position.

The existing multi-pass planning methods (Madsen et al., 2002; Zhang et al., 2011; Yang et al., 2014; Wu et al., 2015; Yan, Ong, & Nee, 2016) are considering the grove geometry as constant where the differences are a result of an error. Only very few studies are systematically handling the groove geometry changes, providing a general solution in multi-pass welding (Yan et al., 2017; Fang et al., 2017).

As the overviewed literature suggests, the weld bead models are mostly given from bead-on-plate experiments. During application on uneven surfaces, the experienced deviations from the expected shapes are considered part of the process's uncertainty and the model's inaccuracy. In multi-pass welding, the unevenness of the layer's surfaces is still neglected, and the bead shapes are approximated with simple geometric forms.

In this paper, a fuzzy system-based empirical model is introduced for the shapes of the weld beads considering the welding process variables and the unevenness of the deposition's surface. The description of the proposed methods (Section 3) is given after the problem definition (Section 2). The model performance and results of the experimental validation are discussed in Section 4. Conclusions are drawn in Section 5.

2. Problem definition

In multi-pass welding, precise positioning of the weld beads in the groove is required to achieve a desirable weld join. The bead shape depends on the previously deposited beads' surface and is directly related to the welding process variables (WPVs). Furthermore, in the parameters' qualified range, multiple combinations of the WPVs can produce the specific weld bead shape (Mishra et al., 2007).

In small and medium-sized enterprises, during the small series production, the process's tuning by trial and error method could take up a significant amount of time. In the planning phase, the beads are deposited layer-by-layer, and their shapes are usually simplified into quadrilaterals – reflecting only the bead size and position (Fig. 1). However, a model describing the relationship between the process parameters and the resulting bead geometry can support selecting the process variables and the automated operation.

A wide range of bead shape models exists to describe a single bead based on the reviewed literature. Excluding those that produce a weld joint from a single bead, most of them are developed from bead-on-plate experiments, where the surface of the base metal plate is evenly flat due to machining. Even in those models applied in additive manufacturing or multi-pass welding, the quality of the base metal surface is neglected. Even though, Li et al. (2018) showed that the base metal's unsymmetrical material distribution is influencing the fluid flow in the melted metal and, consequently, the weld's shape bead after solidification. Still, no model was developed to describe a bead surface formation when deposited on uneven surfaces (Fig. 2). Our proposed model addresses this neglect by including the base metal surface quality besides the WPVs in our model as inputs.

In multi-pass welding one, an important factor is the amount of the deposited material, which can be calculated as A_B^d cross-sectional area of the weld beads from the WPVs.

The theoretical A_B^d cross-sectional area of the weld beads can be estimated according to Eq. (1) by calculating the amount of the deposited weld metal:

$$A_B^d = \frac{\pi D_w^2}{4} \cdot \frac{v_f}{60 v_t}, \tag{1}$$

where v_f represents the wire feed rate, v_t is the torch travel speed and D_w is the feeding wire's diameter. A η_d deposition efficiency can be defined by comparing A_B^d calculated value with the measured bead area, given by the area under the bead surface curve on the given measured cross-section profile. According to (American Welding Society, 2001), the deposition efficiency is above 90 percent during TIG welding. However, the sign and the degree of the deviations might be inconsistent, causing error propagation in multi-pass welding as the layered beads are added on top of each other. The error is usually reduced on a given workpiece by on-site adjustment of the torch position and setting to constant the welding parameters across several layers.

Therefore, we expect that an accurate model utilizing the measurement data can increase the accuracy of the weld bead geometry accuracy. Computational intelligence techniques provide suitable tools to develop such a model. Based on our experience with the bacterial memetic algorithm (BMA) and its competitive performance with other

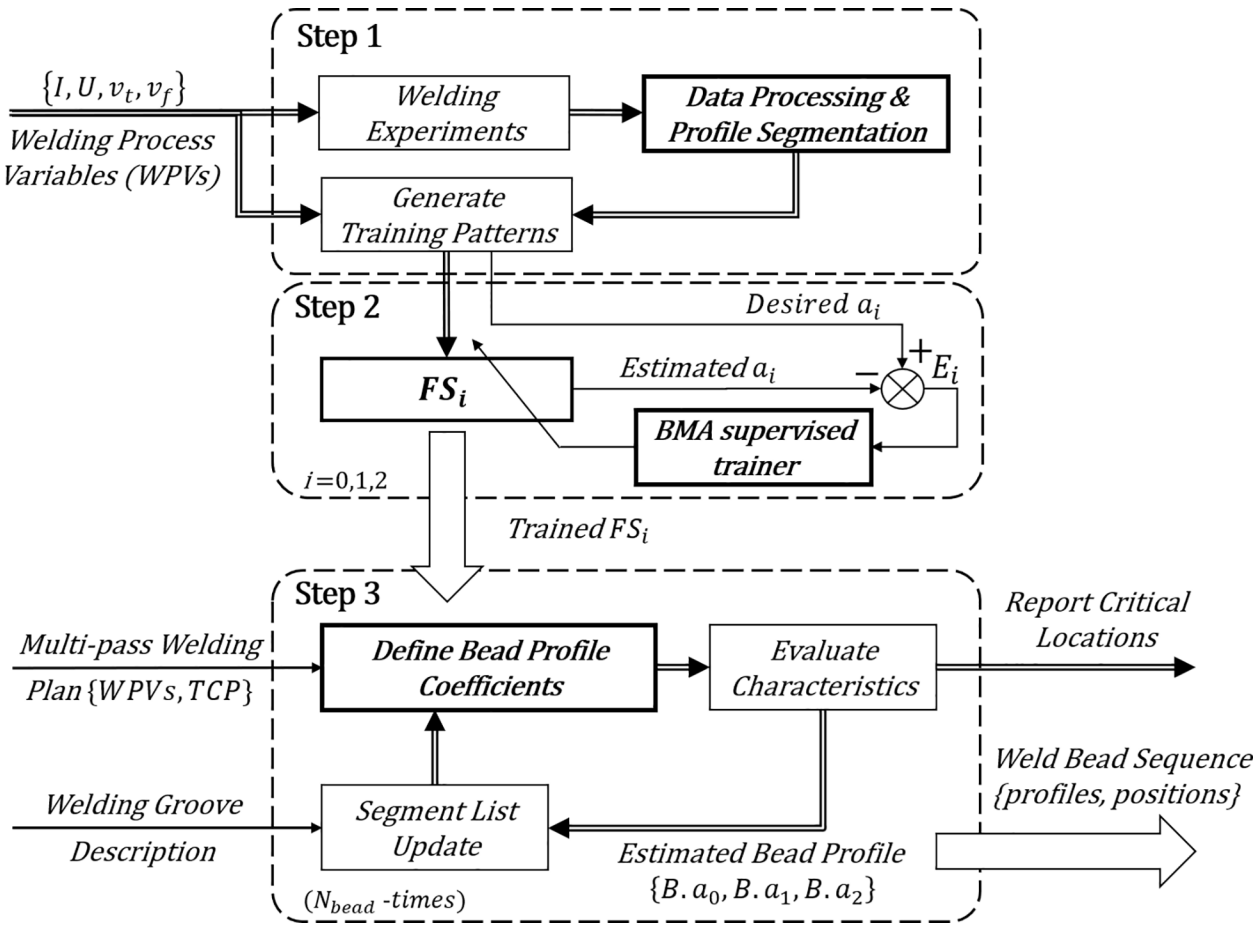

Fig. 3. Overview of the proposed method's structure. The main steps are: Aquisition and processing of the welding data (Step 1.), Weld bead profile modeling (Step 2.), and Application in Multi-pass welding (Step3.).

techniques (Botzheim et al., 2009; Balázs, Botzheim, & Kóczy, 2010; Bódis & Botzheim, 2018), we decided to utilize it and validate its applicability in multi-pass welding.

The objectives of the study are to (i) characterize the unevenness of the base metal surface, (ii) provide the estimation method of weld bead geometry formation on uneven surfaces, and (iii) apply the developed model on 304L stainless steel welding groove.

3. Proposed methods

Our proposed method introduces a modeling method of the weld bead profiles on uneven surface deposition and its application in multi-pass TIG welding. The method's key components are the segmentation and characterization of the base metal surface and the modeling of the weld bead profile function. The base metal surface is handled in segments and approximated with a complete or incomplete second-order polynomial function. The bead profile model consists of fuzzy systems to estimate the coefficients of the bead shape function. The membership functions' parameters are tuned by the bacterial memetic algorithm (Botzheim et al., 2009) during a supervised learning process and evaluated by the Mamdani inference model (Mamdani & Assilian, 1975).

3.1. Overview of the structure

In our method, we are utilizing the weld bead profiles measured by a laser triangulation sensor. The model can be applied even in sensor-less welding applications to estimate the weld bead shapes when deposited on an uneven base metal surface. The overview of the whole modeling and planning process is given in Fig. 3, and can be broken down into the following steps:

Step 1. **Acquisition and processing** of the welding data, provided by the welding experiments and processed by the developed data processing framework (Section 3.2)
Step 2. **Weld bead profile modeling** by tuning the membership functions parameters of the fuzzy systems by BMA in order to infer the coefficients of the bead profile function from the welding process variables and the parameters of the base metal segments (Section 3.3)
Step 3. **Application in Multi-pass welding** of the developed bead model to estimate the bead profile shapes in the iterative bead placement process (Section 3.4)

Welding experiments were carried out on flat plates and in V-grooves to provide the measurement data to develop the empirical model (Section 3.2.1). The welding data were acquired in the form of measured profiles by a laser line triangulation sensor and the WPVs from the welding power source. Additionally, the position and orientation of the tool center were also recorded.

The measurements were aligned and synchronized in the measurement system to provide the organized data for the processing framework (Section 3.2.2). It was represented as weld bead cross sections in the perpendicular plane to the welding direction. Each bead processing took two profile scans of the cross-sections, one without and with the deposited bead. The analysis carried out in situ, the profile features were defined in the workpiece's coordinate system. The final step of the data processing is the generation of the training data (Section 3.2.3) when the base metal- and the bead information is shifted into the weld bead's

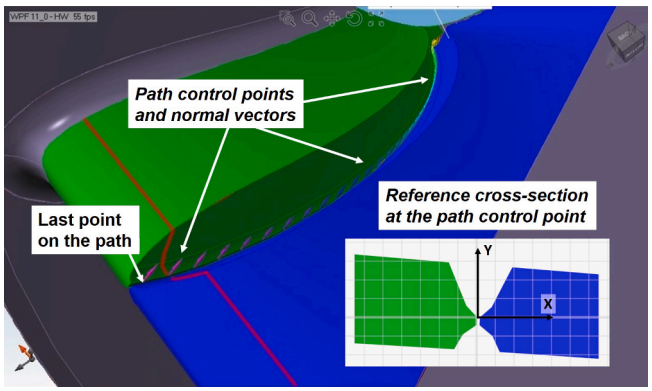

Fig. 4. Digital representation of the welding groove including the root path and a generated cross-section.

local coordinate system.

As the next step, the supervised training was performed by the BMA to realize the weld bead model (Section 3.3). The characteristic points of the trapezoidal membership functions of all rule bases were tuned to reduce the approximation error value (E_i in Fig. 3). The E_i defines the difference between the estimated and the desired value of the function coefficient in the i-th training pattern. All three coefficients of the bead shape function have their fuzzy system, and the bead shape function is given as a combination of them.

The application of the model is embedded in a welding process control system (Section 3.4). It is designed to be applied in a wide range of groove shapes; therefore, the workpiece is defined parametric, while the bead placement is a sequential process.

3.2. Acquisition and processing the welding data

3.2.1. Welding experiments

Bead-in-groove and bead-on-plate welding experiments were carried out to provide the empirical data for the modeling process. In both setup, 304L stainless steel with $40°C$ preheating temperature provided the base metal and 1.2 *mm* diameter *Böhler 13/4-IG* wire the filler material. The experiments were executed in PA welding position, with a regulated constant 12 V and 2.4 *mm* arc gap. The E3 tungsten electrode's diameter was chosen 3.2 *mm* diameter to accommodate the arc current's load. Pure argon provided the shielding gas with a flow rate of $12-14$ L/min.

The bead-on-plate experiments were carried out on a 20 *mm* thick steel plate, clad welded 3 *mm* deep with the filler material. The design of parameters followed an $L_{25}(5^3)$ Taguchi design (Kacker, Lagergren, & Filliben, 1991) layout with a few additional sets to replace the failed combinations. Welding failures happened in the design due to a non-optimal combination of WPVs, such as high heat input with a low wire feed rate or inadequate welding speed selection. Altogether, 33 different WPV combination were included, all of them with two independent trials on a 120 *mm* length.

Bead-in-groove experiments were performed in straight V-grooves. The edges of the 24.5 *mm* thick and 390 *mm* long workpieces were prepared with a 35° bevel angle, 2 *mm* height root faces, and 1 *mm* root gap. Three workpieces were involved in the process, each with a different bead layout containing between 28 and 35 beads.

In the verification process, the same preparation was made both for the flat plates and the welding grooves.

To record the weld bead profiles and the workpieces' surface geometry, the *M2DW 160/40* Line Laser Triangulation Sensor (LTS) was used. Each weld bead was measured by 0.1 *mm* increments along the weld line, which supplied the raw data cross-sections for further data processing. The first and the last fifth of the weld beads were neglected; thus, only the stabilized cross-sectional area was considered. The multi-pass welding experiments excluded the root pass since the welding conditions are well defined and strictly controlled due to its critical impact on the final joint quality. The exported measurement data included – besides the profile points – the recorded tool center points and the actual values of the WPVs.

3.2.2. Profile segmentation and data processing

A framework was developed in LabVIEW™ to process the bead profiles' measurements, as the pseudo-code of the whole process is shown in Algorithm 1. The measurement data imported from the measurement system on the workpiece level, containing each weld bead and all the measured cross-sections.

Algorithm 1.: Processing of the bead profile measurements

```
Data: Weld Bead Profile Measurements
Input: N_trials, N_profiles[ID_trial]
1  for Each workpiece do
2      for Each weld bead do
3          Merge cross-sections into combined profiles;
4          for Each combined profiles do
5              Filter measurement and correct errors;
6              Profile Segmentation;
7              Curve fitting;
8              Acquire bead characteristics;
9          end
10     end
11     Postprocessing;
12     Export Training patterns;
13     Export Bead characteristics;
14 end
```

The welding groove can be given in a CAD data file, a profile scan of the groove, or a combination of those two (Fig. 4). Additionally, the root path definition is also required to provide the robot trajectory reference points and the path normal-vectors. In each path point, the right-handed local coordinate system is defined by the normal-vector (directing towards the groove's opening) as the y-axis and the vector directing towards the next path point as the z-axis. The characteristic cross-sections are defined at the path points in the $x-y$ plane along the root path. The groove's mathematical description is made for each characteristic cross-section from the digital representation of the workpiece.

The right-left part of the workpiece is considered according to the x-axis of the local coordinate systems, the positive x interval defines the right side, and the negative is the left. The segments' describing functions are approximated by a second-order polynomial for unified description and a defined integral value in the coordinate system of $x-y$ plane, where the x is the running variable. In a complex groove geometry, the groove slope function can be sectioned into several segments, described by elementary functions. In that case, the groove slope function became their superposed function, and the elementary functions should be used in their range of interpretation.

Upon loading the measurement data (Algorithm 1, ln.3), the individual cross-sections were merged into processible sections defined by the desired resolution along the weld line – 5 *mm* thick sections in the recent application. The unified cross-sections were filtered by removing the measurement errors and applying a median filter of rank two and a second-order derivative filter. The unification of the cross-sections performed for each bead in the groove, therefore maintaining the profiles' indexing. After the filtering, the base metal and the bead profiles are aligned, removing any remained distortion of the measurements and unification.

The next step in the process is the segmentation of the measured profiles (Algorithm 1, ln.6). First, the difference between the base metal and the bead profile is examined to locate the bead center's approximated position and the toe points. Second, the main features are identified, such as the top surface of the workpiece, the groove faces, and the deposited beads' uneven surface. Third, the individual beads and bead fractions are located according to the given number of visible bead

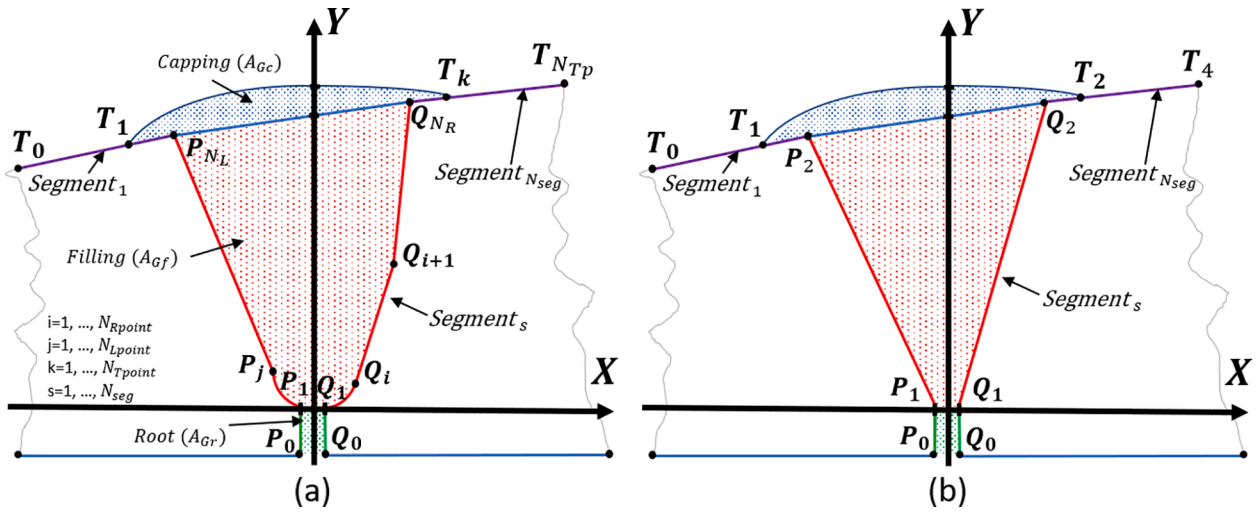

Fig. 5. Definition of the characteristic points and the coordinate system on a (a) general groove and a (b) V-groove cross-section. Segments are defined between the characteristic points of the groove features – *T* points are on the top surface, *P* and *Q* points are located on the left and the right side of the groove.

segments. The feature extraction is based on the first and second derivatives of the given profile points. It is approximated from the given points' linear regression and its surrounding points in a given radius.

The profile points are then handled separately, and for each segment, the fitting curve is defined: linear fitting for the straight features and polynomial fitting for the bead segments. From that point, the profile is represented as a list of segmented features – each containing the type definition, the coefficients of the fitting curve, and the intersection point with the subsequent segment.

Fig. 5 illustrates a generalized, mathematical description of the groove geometry. Segments are defined between the groove features' characteristic points – *R* points are on the top surface, *P* and *Q* points are located on the left and the right side of the groove, respectively. The N_{Rpoint} and N_{Lpoint} number of points are typically between two and four depending on the edge preparation. If the groove is a V-groove with a straight groove face, then there is no internal breakpoint; otherwise, the root radius (U-groove) and additionally, beveling defines more. Similarly, N_{Tpoint} defines the number of characteristic points on the top surface, thus the number of segments.

When all segments were identified, the bead characteristics are calculated (Algorithm 1, ln.8). The processing framework allows us to manually adjust the segment borders, which, after the confirmed modifications, would update the whole segment list and the corresponding curve coefficients.

Fig. 2 depicts a general weld bead in a groove and the bead characteristics defined according to the image. These are namely: the area of the bead cross-section (A_B), the coordinates of the bead center (*BC*), toe points (T_1 and T_2), and the contact angles at the toe points (Φ_1 and Φ_2).

The S_i base metal segments are the earlier deposited bead surfaces or the groove edges. The points positions are given in *mm* in the Descartes coordinate system (in the workpiece coordinate system and the bead's local coordinate system), the contact angles are in *rad*. The area of the weld bead is calculated as

$$A_B = \int_{T_1}^{T_2} f_B \mathrm{d}x - \sum_{i=1}^{N_{subs}} \int_{I_{i-1}}^{I_i} f_{S_i} \mathrm{d}x, \tag{2}$$

where $T_1 = I_0$ and $T_2 = I_{N_{subs}}$ are the toe points (intersection points of the first and the last segments and the bead shape function, respectively), the points I_1 to $I_{N_{subs}-1}$ are the intersection points of the adjacent segments, f_B is the bead shape function, f_{S_i} is the shape function of the *i*-th segment. Both f_B and f_{S_i} functions are given in the second order polynomial form

$$f_B = B.a_0 + B.a_1 \cdot x + B.a_2 \cdot x^2 \tag{3}$$

$$f_{S_i} = S_i.a_0 + S_i.a_1 \cdot x + S_i.a_2 \cdot x^2 \tag{4}$$

The last step is post-processing (Algorithm 1, ln.11), when the whole bead is analyzed, and an overview is given about the bead characteristics features for each cross-section in graphical form. The system automatically detects if any of the evaluated characteristics are out of the acceptable range and marks the corresponding cross-section to be excluded from the export list. The range of acceptance is defined around the mean value of the given characteristics of the exportable cross-section.

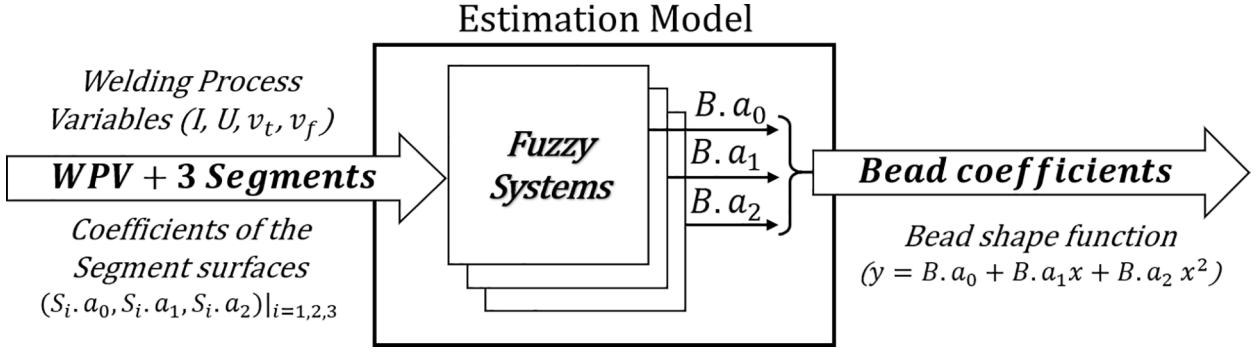

Fig. 6. The inputs and outputs of the fuzzy systems as the key component of the weld bead shape model.

Table 1
Ranges of the Parameters.

Input Name	Notation	Min value	Max value	units	Output Name	Notation	Min value	Max value	units
Arc current	I	180	260	$[A]$	Bead a_0	$B.a_0$	0.5700	3.2426	$[-]$
Arc voltage	U	11.3	13.9	$[V]$	Bead a_1	$B.a_1$	−1.1876	1.1876	$[-]$
Torch travel speed	v_t	1.9	3.0	$[mm/s]$	Bead a_2	$B.a_2$	−0.2983	0.10522	$[-]$
Wire feed rate	v_f	500	1900	$[mm/min]$	Bead width	w	5.1	13.6	$[mm]$
Segment-1 a_0	$S_1.a_0$	−8.5490	2.3304	$[-]$	Bead area	A_B	2.8	16.3	$[mm^2]$
Segment-1 a_1	$S_1.a_1$	−1.7163	0.41421	$[-]$	Toe-1 X-coordinate	$T_1.X$	−7.9	−1.3	$[mm]$
Segment-1 a_2	$S_1.a_2$	−0.17121	0.16982	$[-]$	Toe-1 Y-coordinate	$T_1.Y$	−2.8	3.3	$[mm]$
Segment-2 a_0	$S_2.a_0$	−0.18400	0.11662	$[-]$	Toe-2 X-coordinate	$T_2.X$	1.3	7.9	$[mm]$
Segment-2 a_1	$S_2.a_1$	−1.3061	1.3061	$[-]$	Toe-2 Y-coordinate	$T_2.Y$	−2.8	3.3	$[mm]$
Segment-2 a_2	$S_2.a_2$	−0.38309	0.53976	$[-]$	Contact angle-1	Φ_1	1.0711	3.2035	$[rad]$
Segment-3 a_0	$S_3.a_0$	−8.5491	2.3304	$[-]$	Contact angle-2	Φ_2	1.0711	3.2035	$[rad]$
Segment-3 a_1	$S_3.a_1$	−0.41421	1.7163	$[-]$					
Segment-3 a_2	$S_3.a_2$	−0.17121	0.16982	$[-]$					

3.2.3. Generating training data for modeling

During the data export, besides the training data, the processed state of each cross-section is exported. Thus when the beads are re-evaluated, the already defined results are presented in the program. Furthermore, an overview is tabulated into a.csv file format to reference the training performance evaluation. The above-described process is carried out for each bead in the welding groove and all workpieces included in the model development.

The weld bead shape model is structured as multiple-input–single-output. The inputs are the four WPVs and the coefficients of the segment functions ($S_i.a_0$, $S_i.a_1$, and $S_i.a_2$), altogether 13 parameters. The outputs are the coefficients of the bead shape function ($B.a_0$, $B.a_1$, and $B.a_2$) – each parameter is estimated by its fuzzy system (Fig. 6). Three WPVs were selected to be controlled to comply with the industrial aspect of the application, namely the arc current (I), the torch travel speed (v_t), and the wire feed rate (v_f). Additionally, as a recorded input value, the arc voltage (U) was also included because its small fluctuation still significantly affected the heat input. The parameter ranges are tabulated in Table 1, where the first column contains all the model's inputs, and the second column the outputs. The bead shape coefficients are extended with the list of the bead's characteristic parameters, where the ranges are interpreted for the measured values.

In the literature, several curvature descriptions are given to describe the shape function of the weld bead. However, the parabola shape was chosen because of its ability to characterize the segments generally in the welding groove. The bead profiles and straight lines can be given with only three parameters while a segment given with the root radius can be approximated with an acceptably small error.

The values of the a_i coefficients in the parabola function, given as

$$a_0 + a_1 \cdot x + a_2 \cdot x^2, \tag{5}$$

define the type of curve. If all a_i coefficients are non-zero, then it is a general parabola, if only $a_1 = 0$, then it is a symmetrical one (the beads in the flat plate experiment described mostly like that). The case of $a_2 = 0$ describes a straight line, and if both a_1 and a_2 are zero, then it is a horizontal line, crossing the y-axis at a_0. Such horizontal lines are describing the top surfaces of the grooves and the flat plates.

The segmented base metal, including all the groove's visible features and the previously deposited beads, is represented as a list of coefficients of the segments, with the type definition and the intersection point's x coordinate with the subsequent segment.

3.3. Bacterial memetic algorithm for training fuzzy systems

The weld bead shapes' modeling is carried out utilizing fuzzy systems for the describing curve function's coefficients. To define the fuzzy systems, the BMA was applied as a supervised trainer (Step 2. in Fig. 3) on the $N_{pattern}$ training patterns. The operations are carried out on the **b** bacterium, each encoding the fuzzy rules in their chromosomes (Botzheim et al., 2009) as a $\mathbf{b}_k$ vector (k is the iteration variable of the individuals).

The rules in the fuzzy system are given in the following form:

$$Rule_i: \text{ IF} x_1 = A_{i,1} \text{ and } \ldots \text{ and } x_n = A_{i,n} \text{ THEN } y = B_i,$$

where $\mathbf{x} = (x_1, \ldots x_n)$ is the input vector, y is the output, $A_i = (A_{i,1} \ldots A_{i,n})$ is the antecedent parameter vector, and B_i is the consequent parts in the i-th rule. The rule base is defined to cover the whole interval of interpretation of the input variables to provide a valid inference result. Trapezoidal typed membership functions are used which can be written in the following form:

$$\mu_{A_{ij}}(x_j) = \begin{cases} \dfrac{x_j - a_{ij}}{b_{ij} - a_{ij}}, & \text{if } a_{ij} < x_j \leqslant b_{ij} \\ 1, & \text{if } b_{ij} < x_j \leqslant c_{ij} \\ \dfrac{d_{ij} - x_j}{d_{ij} - c_{ij}}, & \text{if } c_{ij} < x_j \leqslant d_{ij} \\ 0, & \text{otherwise} \end{cases} \tag{6}$$

In this equation $a_{ij} \leqslant b_{ij} \leqslant c_{ij} \leqslant d_{ij}$ denote the four breakpoints of the membership function belonging to the i-th rule and the j-th input variable. The output membership function in the i-th rule is also described as a trapezoid where the breakpoints are denoted as a_i, b_i, c_i, d_i (Eq. (7)).

$$\mu_{B_i}(y) = \begin{cases} \dfrac{y - a_i}{b_i - a_i}, & \text{if } a_i < y \leqslant b_i \\ 1, & \text{if } b_i < y \leqslant c_i \\ \dfrac{d_i - y}{d_i - c_i}, & \text{if } c_i < y \leqslant d_i \\ 0, & \text{otherwise} \end{cases} \tag{7}$$

As in the original Mamdani algorithm, the minimum operator is used as the t-norm in the inference mechanism, meaning that the degree of matching of the i-th rule in the case of an N_{input}-dimensional crisp **x** input vector is:

$$w_i = \min_{j=1}^{N_{input}} \mu_{A_{ij}}(x_j). \tag{8}$$

The output of the fuzzy inference is then:

$$y(\mathbf{x}) = \frac{1}{3} \frac{\sum_{i=1}^{N_{rule}} 3w_i(d_i^2 - a_i^2)(1 - w_i) + 3w_i^2(c_i d_i - a_i b_i) + w_i^3(c_i - d_i + a_i - b_i)(c_i - d_i - a_i + b_i)}{\sum_{i=1}^{N_{rule}} 2w_i(d_i - a_i) + w_i^2(c_i + a_i - d_i - b_i)}. \tag{9}$$

The number of rules is N_{rule}, and N_{input} is the number of input dimensions.

By adjusting the breakpoints of the fuzzy rules' trapezoids, the algorithm carries out the minimization of the $E(\mathbf{b}_k)$ cumulative error, defined as the 2-norm sum of squared $\mathbf{e}_k$ error of the $d^{(p)}$ desired and the $y_k(\mathbf{b}_k, \mathbf{x}^{(p)})$ model's output value. The output of the fuzzy rule bases is evaluated – in each step of the BMA and for all the bacteria – according to the Mamdani Inference Model for the $\mathbf{x}^{(p)}$ inputs as the p-th training pattern.

Algorithm 2.: Bacterial memetic algorithm

Data: $N_{pattern}$ training patterns
Input: $Parameters$: N_{ind}, N_{gen}, N_{rule}, N_{clone}, l_{bm}, M_{unit}, LM_{prob}, LM_{iter}, γ_{init}, τ, N_{inf}, l_{gt}, I_{unit}

Create initial population;
for $gen = 1$ *to* N_{gen} **do**
  for $ind = 1$ *to* N_{ind} **do**
    `/* Bacterial mutation */`
    Create $(N_{clone} + 1)$ clones of B_{ind};
    for $seg = 1$ *to* $N_{segment}$ **do**
      Select l_{bm} number yet unmutated random genes;
      for $j = 1$ *to* N_{clone} **do**
        Mutate selected genes in $Clone_j$
      end
      for $k = 1$ *to* $N_{clone} + 1$ **do**
        Evaluate $Clone_k$ using Eq. (10)
      end
      Select $BestClone$;
      Transfer best clone's gene to all clones;
    end
    Set $B_{ind} = BestClone$;
    `/* Levenberg-Marquardt algorithm */`
    if $Random(probability) < LM_{prob}$ **then**
      $k = 1$;
      while $k < LM_{iter}$ **and** $\tau_k > \tau$ **do**
        Calculate $\mathbf{J}(\mathbf{b}_k)$ Jacobi matrix as Eq. (13);
        Calculate $\mathbf{s}_k$ update vector as Eq. (14);
        Calculate r_k trust region as Eq. (15);
        Calculate γ_{k+1} bravery factor as Eq. (16);
        Evaluate the update vector's effect as Eq. (17);
        Calculate τ_k stopping criteria;
        $k = k + 1$;
      end
    end
    `/* Gene transfer in the population */`
    for $inf = 1$ *to* N_{inf} **do**
      Ascending order of the population according to Eq. (10);
      $B_{source} = Random(0, ..., N_{ind}/2 - 1)$;
      $B_{destination} = Random(N_{ind}/2, ..., N_{ind})$;
      Select random l_{gt} genes;
      Transfer the selected genes from B_{source} to $B_{destination}$;
    end
  end
end

Table 2
Parameters of the BMA

Parameter Name	Notation	Value
Number of inputs	N_{input}	13
Number of patterns	$N_{pattern}$	5458
Number of rules	N_{rule}	2 – 12
Number of generations	N_{gen}	50
Number of individuals	N_{ind}	50
Number of clones	N_{clone}	3
Mutation unit	M_{unit}	point
Mutation segment length	l_{bm}	1
Probability of LM[1]	LM_{prob}	40
Max. LM iteration step	LM_{iter}	8
Bravery factor (initial)	γ_{init}	1.00
Terminal condition	τ	0.0001
Number of infections	N_{inf}	50
Infection unit	I_{unit}	rule
Infection segment length	l_{gt}	1

[1] Levenberg–Marquardt algorithm

$$E(\mathbf{b}_k) = ||\mathbf{e}_k||_2^2 \tag{10}$$

$$\mathbf{e}_k = [e_k^{(p)}] = [d^{(p)} - y_k(\mathbf{b}_k, \mathbf{x}^{(p)})] \tag{11}$$

Algorithm 2 shows the pseudo-code of the BMA and in Table 2 the applied meta parameters are listed. The BMA consists of three main calculation steps: the *Bacterial mutation*, the *Local search*, and the *Gene transfer*. The iterative process is performed the number of generations (N_{gen}) times, starting with an initial population containing N_{ind} random individuals applying the predefined (N_{rule}) number of rules. Thus, in the initial population creation, the total number of the created membership functions is $N_{ind}\cdot(N_{input}+1)\cdot N_{rule}$ where $N_{input} = 13$ is the number of input variables and each membership function has four parameters to maintain their trapezoidal characteristics.

In each generation, the *Bacterial mutation* and the *Local search* are applied to each individual, and the *Gene transfer* on the whole population at once.

3.3.1. Bacterial mutation

In the *Bacterial mutation* step, the bacteria and its N_{clone} clones are subjects of random changes in their genes, which according to the M_{unit} mutation unit can either be a point (breakpoint of the trapezoid), a membership function (trapezoidal, four points), or an entire rule. In each iteration, N_{clone} clones are created then the random changes are performed. The number of modified genes is given by the l_{bm} mutation segment length. After that, all the clones are evaluated, the best clone transfers the mutated part into the other clones, and in the end, only the best rule base is kept. The *Bacterial mutation* is repeated $N_{segment}$ times, where

$$N_{segment} = 4\cdot N_{rule}\cdot(N_{input}+1)/l_{bm} \tag{12}$$

in the case when point mutation is applied (M_{unit} is set to point).

3.3.2. Levenberg–Marquardt algorithm

The *Local search* in BMA was utilizing the Levenberg–Marquardt algorithm and carried out with a LM_{prob} probability for each individual until the complex $\tau_k < \tau$ (Botzheim et al., 2009) terminal condition is met or the maximum LM_{iter} number of iteration steps is reached.

Let denote $\mathbf{J}(\mathbf{b}_k)$ the Jacobian matrix of bacterium $\mathbf{b}_k$:

$$\mathbf{J}(\mathbf{b}_k) = \left[\frac{\partial y_k(\mathbf{b}_k, \mathbf{x}^{(p)})}{\partial \mathbf{b}_k^T}\right], \tag{13}$$

where each row of the $\mathbf{J}(\mathbf{b}_k)$ matrix contains the partial derivatives of the bacterium $\mathbf{b}_k$ encoded fuzzy system's output calculated for the given $\mathbf{x}^{(p)}$ input training pattern. The detailed definitions of the derivatives and the calculation steps are given in Botzheim et al., 2009.

In the Levenberg–Marquardt algorithm, the approximation towards the local minimum is defined by the $\mathbf{s}_k$ update vector, r_k trust region, and γ_k bravery factor.

$$\mathbf{s}_k = -(\mathbf{J}^T(\mathbf{b}_k)\mathbf{J}(\mathbf{b}_k) + \gamma_k\mathbf{I})^{-1}\mathbf{J}^T(\mathbf{b}_k)\mathbf{e}_k, \tag{14}$$

$$r_k = \frac{E(\mathbf{b}_k) - E(\mathbf{b}_k + \mathbf{s}_k)}{E(\mathbf{b}_k) - ||\mathbf{J}(\mathbf{b}_k)\mathbf{s}_k + \mathbf{e}_k||_2^2} \tag{15}$$

The value of γ_k bravery factor controls both the search direction and the magnitude of the update – adjusted dynamically depending on the value of the r_k trust region. If the value of γ_k converges towards zero, then the algorithm applies the Gauss–Newton method; if towards infinite, the algorithm gives the steepest descent approach.

$$\gamma_{k+1} = \begin{cases} 4\cdot\gamma_k & \text{if } r_k < 0.25 \\ \gamma_k/2 & \text{if } r_k > 0.75 \\ \gamma_k & \text{otherwise} \end{cases} \tag{16}$$

The local search is evaluated as successful if the update vector modifies the bacterium towards the local minimum. In this case, the bacterium's new value is carried on; otherwise, it is left unchanged.

$$\mathbf{b}_{k+1} = \begin{cases} \mathbf{b}_k + \mathbf{s}_k & \text{if } E(\mathbf{b}_k + \mathbf{s}_k) < E(\mathbf{b}_k) \\ \mathbf{b}_k & \text{otherwise} \end{cases} \tag{17}$$

3.3.3. Gene transfer

The last operation in a generation is the horizontal *Gene transfer*, allowing the recombination of genetic information between two bacteria. This operation is performed N_{inf} number of infection times per generation. The individuals are organized into ascending order according to their E error value then split into halves representing the better and the worse individuals. During the infection, a randomly chosen, better bacteria overwrites a randomly chosen, worse one's gene with its own I_{unit} infection unit time l_{gt} infection segment length. The infection unit here may be defined in the same ways as the M_{unit} mutation unit. When the *Gene transfer* operation is finished, the new generation's execution starts until the predefined number of generations (N_{gen}) is performed.

3.4. Application in multi-pass bead positioning

During the application of the developed bead shape estimation model, an iterative process is carried out to place the weld beads in the welding groove sequentially. The pseudo-code of this placement process is presented in Algorithm 3. The operation requires the description of the welding groove (according to Section 3.2.2) and the *Welding Plan*, containing the information about the WPVs and the tool center point (TCP) for each N_{bead} weld bead. If the welding plan were the desired output, the additional rules of bead positioning and WPVs selection would be necessary, which requires further discussion but not part of this article.

Table 3
Possible selection of the segment from the base metal segment list (index 0 is the segment containing the bead center)

Case	Segment–1	Segment–2	Segment–3
0	−1	0	+1
1	0	0	0
2	−1	0	0
3	0	0	+1
4	−2	−1	0
5	0	+1	+2

For simplicity, we assume that the *Welding Plan* is available.

Algorithm 3.: Model application in multi-pass welding

Data: Bead Shape Estimation Model
Input: $WeldingPlan[N_{bead}][WPVs, TCP]$, *Groove*

1 $Segmentlist$ Initialization from *Groove*;
2 **for** $bead = 1$ *to* N_{bead} **do**
3 Acquire *BeadCenter*;
4 Define probable $SegmentCombinations$;
5 **for** $scomb = 1$ *to* $SegmentCombinations$ **do**
6 Acquire $B.a_0$, $B.a_1$, and $B.a_2$ bead shape coefficients;
7 **end**
8 Select best combination of the coefficients;
9 Evaluate bead characteristics;
10 Update segment list;
11 **end**

In the initialization, the *Groove* description provides the initial list of the segments. The process starts with the acquisition of the *BeadCenter*, defined as the intersection of the center-line of the welding torch (going through the TCP) and the base metal's surface. Based on the given bead center, the list of the probably *SegmentCombinations* can be selected since there is no information about how wide the weld bead will be; thus, it can stretch over multiple segments or remain within one segment's borders.

Since three adjacent segments need to be entered, the proper combination should be selected (Algorithm 3, ln 4.), as shown in Table 3. One segment (index 0) is fixed as it contains the bead center, but the two sides need some consideration. As the most common scenario, the previous and the following segments are selected (case 0). If the bead is too small, or the given base metal segment is large, the two sides would be the same as the middle segment (case 1). On the other hand, the bead can be deposited asymmetrically like one side is still on the center's segment, and the other one is on an adjacent segment (cases 2 and 3). In the unlikely event that the adjacent bead is small, the bead's side would stretch over the second segment (cases 4 and 5).

The *Segment Combinations* with the WPVs can be entered into the previously developed model to acquire the $B.a_0, B.a_1, B.a_2$ coefficients of the bead surface function.

When the bead model is applied and fed with the segment information, all the cases mentioned earlier are given, then the resulting bead shape is evaluated (Algorithm 3, ln 8.). The cases fulfilling the criteria that the segments' index containing the toe points match the fed segments' indices are kept the other cases are neglected. If multiple satisfactory combinations are found, the priority is given to those which toe points are closer to the *Bead Center* and covering an area with less difference to the expected bead area.

The characteristics of the newly acquired bead can be evaluated now. The exact shape allows us to perform manufacturing-critical analysis of the process and highlight the bead's problematic locations, thus eliminating the welding defects. A good measure is to monitor the Φ_1 and Φ_1 contact angle values. If a too-narrow gap is created, the fusion could be incomplete, gas pockets or slag inclusions could appear.

In the last step of the planning process (Algorithm 3, ln 10.), when the new bead is defined, the segment list is updated to include it and remove the fully covered segments or those whose remaining length became neglectable. The iterations are repeated until all weld bead is deposited.

4. Results and discussion

In the following, the development work results will be discussed, including the overview of the main findings of the modeling process of the weld bead profiles. The performance of the development model was compared with a statistical model (multi regression analysis, MRA) models, and over cross-validation, too. Furthermore, demonstration and evaluation of the application cases are presented.

The trained model's performance was evaluated by comparing the estimated and the measured values to define the goodness of the fitting using the root mean square error (RMSE). The RMSE values were given for the bead geometry with the bead shape function defined by the estimated coefficients and compared with the measurements. Beside the direct comparison of the $B.a_0, B.a_1$, and $B.a_2$ coefficients; the calculated values of the A_B bead area, w bead width, location of the T_1 and T_2 toe points and the three-phase contact angle (Φ) values were considered. The value of the toe points' positioning error is calculated as the distance between the estimated and the measured locations. Similar comparisons were carried out for a separate set of validation data.

The data sets for the training and validation were extracted from the welding experiments. The processing of the cross-sections of the weld beads and the base metal provided the patterns. The patterns were generated two ways for each cross-section since they could be seen from two views – a straight view and a mirrored one. Therefore, the double amount of pattern could be used in the model's tuning because the segments' descriptions were not symmetric, thus containing additional information for the model. The mirrored pattern generation required to negate the value of the a_1 coefficients of each function (both the base metal's and the bead's), then swapping all coefficients' position of *Segment–1* and *Segment–3*. The WPVs of the pattern was left unmodified. The mirroring was only necessary to be performed on the patterns generated from the cross-sections of beads deposited in the welding groove.

One of the mirrored views of the three workpieces was selected as validation data. The fitting evaluation was carried out on each bead and cross-section individually, the multi-pass validation on the whole filled groove. Altogether, 5458 different bead cross-section was used during the training and 947 bead cross-section in the validation data set.

During the data processing, some of the bead cross-section failed to be processed and distorted the later results. Therefore, a filter was applied, based on the expected bead area, as discussed in Section 2. The deposition efficiency may vary depending on the WPVs, but while filtering the measurement and estimation data, the lossless value is set as the reference deposited cross-sectional area. Both the measured and estimated data were filtered according to the deviation from the reference area, where the threshold set to arbitrary ± 0.3. The wide threshold range was chosen only to remove the clearly outlying data points. Over the set threshold limit, the data point was considered faulty due to some unforeseen errors in the processing system. This filtering method can also be used during the model's application since the WPVs values are typically defined beforehand.

4.1. Multiple regression analysis model

Multiple regression analysis was performed to create a reference model to our method since no similar model exists in the overviewed literature. The regression model data sets were the same as were used for training and validating our machine learning models. The extracted regression coefficients for coefficients of the bead shape function are tabulated in Table 5. The coefficients with the significant effect (level of significance is $p \leq 0.05$) on the modeled output were marked with an

asterisk, next to the p-value. Since each input parameter has a significant effect on at least one output parameter, none of them can be excluded from the modeling. The coefficient of determination (R^2) as calculated for each output parameter are: 0.889 for $B.a_0$, 0.793 for $B.a_1$, and 0.677 for $B.a_2$.

The calculated RMSE values for the training and validation are presented in the first row of Table 4.. The goodness of fitting is visualized in Fig. 7 with yellow rhomboid markers by plotting the comparison of the estimated and the measured coefficients, and additionally, the bead cross-sectional area. Both in the training and the validation, the MRA model provided a sufficient fitting for the data, verifying the data set's coherency. However, the best performing BMA trained fuzzy system (marked by blue squares) outperforms the MRA model during the validation. Furthermore, as shown later, most of the examined model by BMA would have better fittings than the MRA model.

Table 4
RMSE values of the MRA model for the training and the validation.

RMSE	$B.a_0$	$B.a_1$	$B.a_2$
Training	0.1122	0.0858	0.0194
Validation	0.2171	0.1791	0.0217

4.2. Evaluation of the trained fuzzy systems

The fuzzy systems were trained with a different number of rules, set between two and twelve. The required calculation time depended on the number of rules since they defined the number of segments in the bacteria's chromosomes (see Eq. 12). In the case of two rules, the number of segments is 112, while for twelve rules, it is 672. The computations of the fuzzy systems were carried out on a PC using an Intel® Core™ i7-5820 K Processor at 3.30 GHz and an NVIDIA GeForce® GTX 970

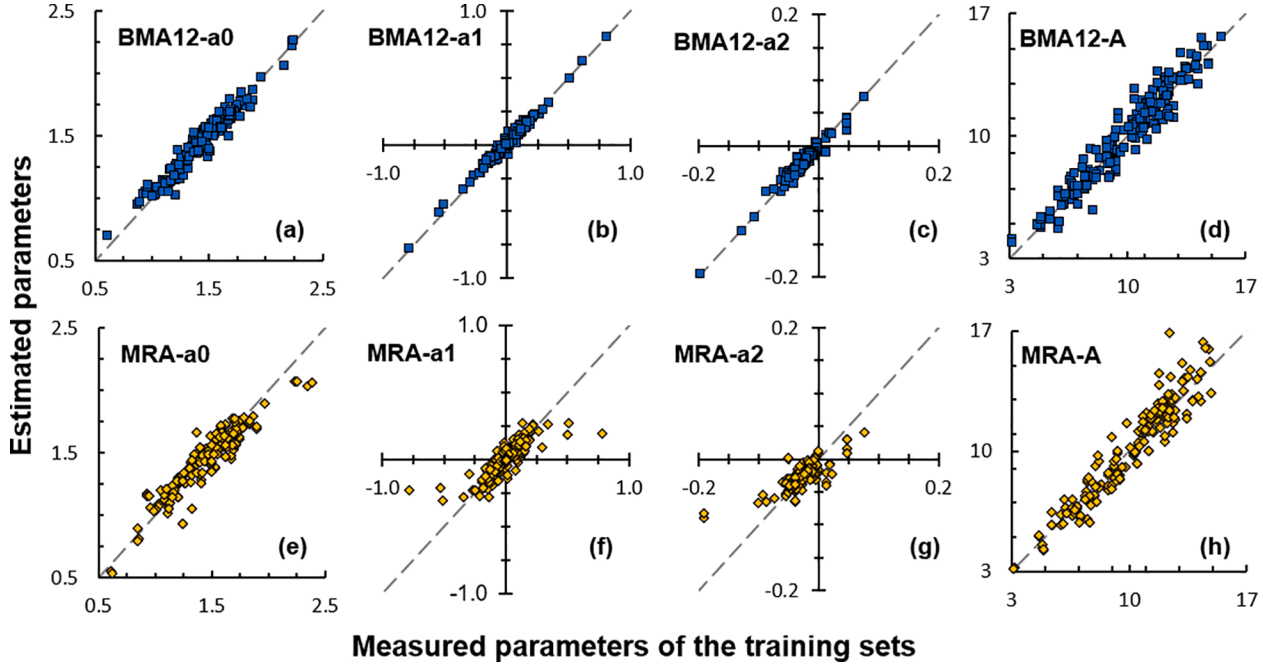

Fig. 7. Fitting plots of the estimated and measured coefficients of the bead shape function and bead area. (a) – (d) parameters estimated by the BMA model utilizing 12 fuzzy rules for the training data, (e) – (h) parameters estimated by the MRA model for the training data.

Table 5
MRA model coefficients to estimate the $B.a_0, B.a_2$, and $B.a_2$ coefficients of the weld bead function.

	$B.a_0$			$B.a_1$			$B.a_2$		
Name	Coefficient	p-value		Coefficient	p-value		Coefficient	p-value	
Intercept	2.6193	0.0000	*	0.0032	0.9793		-0.1501	0.0000	*
Arc current	-0.0031	0.0000	*	0.0002	0.1722		0.0004	0.0000	*
Arc voltage	-0.0941	0.0000	*	0.0019	0.8537		0.0042	0.0756	
Torch travel speed	-0.2585	0.0000	*	-0.0209	0.0211	*	-0.0053	0.0112	*
Wire feed rate	0.0009	0.0000	*	0.0000	0.2037		0.0000	0.0000	*
Segment-1 a_0	0.1442	0.0000	*	-0.0424	0.0000	*	0.0062	0.0000	*
Segment-1 a_1	-0.4189	0.0000	*	0.2140	0.0000	*	-0.0309	0.0000	*
Segment-1 a_2	0.0625	0.5926		1.1911	0.0000	*	-0.0596	0.0040	*
Segment-2 a_0	-0.1954	0.1033		0.0728	0.4275		0.5881	0.0000	*
Segment-2 a_1	-0.0086	0.3811		0.2592	0.0000	*	0.0074	0.0000	*
Segment-2 a_2	-0.1260	0.0242	*	0.0090	0.8330		0.3161	0.0000	*
Segment-3 a_0	0.1540	0.0000	*	0.0401	0.0000	*	0.0076	0.0000	*
Segment-3 a_1	0.4449	0.0000	*	0.2066	0.0000	*	0.0299	0.0000	*
Segment-3 a_2	-0.5144	0.0000	*	-1.1732	0.0000	*	-0.1109	0.0000	*

Table 6
Comparison of the RMS Error values of training data between measurements and estimations of the different models.

Model	Profiles	w	A_B	$T_1.X$	$T_1.Y$	$T_2.X$	$T_2.Y$	Φ_1	Φ_2
MRA	5370	0.87	1.03	0.61	0.33	0.64	0.32	0.1317	0.1239
BMA-R02	4996	1.13	1.75	0.80	0.28	0.70	0.26	0.1316	0.1279
BMA-R03	5196	0.97	1.42	0.69	0.21	0.68	0.24	0.0976	0.1064
BMA-R04	5210	0.76	1.11	0.58	0.24	0.55	0.22	0.0893	0.0897
BMA-R05	5236	0.77	1.14	0.54	0.21	0.58	0.18	0.0903	0.0857
BMA-R06	5259	0.71	1.00	0.54	0.17	0.51	0.21	0.0798	0.0806
BMA-R07	5330	0.68	1.02	0.53	0.18	0.47	0.17	0.0780	0.0776
BMA-R08	5351	0.73	1.03	0.50	0.19	0.50	0.18	0.0790	0.0791
BMA-R09	5363	0.69	1.06	0.48	0.15	0.50	0.17	0.0712	0.0757
BMA-R10	5345	0.64	0.92	0.48	0.17	0.48	0.16	0.0703	0.0736
BMA-R11	5375	0.69	0.98	0.48	0.14	0.51	0.16	0.0706	0.0781
BMA-R12	5369	0.66	0.90	0.44	0.14	0.49	0.21	0.0693	0.0740

graphics card. For two rules, calculation of one generation for each coefficient took 10.2 s, 93.6 s for eight rules, and 251.9 s for twelve rules on average. The exact time of a generation varied based on how many local searches were carried out since this calculation step performed with LM_{prob} probability per bacterium. Retrieving a value utilizing the fuzzy system took only a few milliseconds. However, the fuzzy rules are not intended to use in a real-time system. Therefore, their response time is not critical but is required to be quick enough for comfortable usage.

The best performing model was the fuzzy systems with twelve rules for each coefficient. The exact rules are presented in the Appendix, tabulated in Table A.1, A.2, A.3. On the training data set, Table 6 shows the RMS Error values of the different setups. As the number of rules increases, the estimation error decreases; thus, a better approximation is given with a higher number of rules. Moreover, the number of removed cross-sections (Table 6 "Profiles" column) remains around two percent above six rules, similar to the MRA model. Estimating two out of the three coefficients is better for already with two rules (BMA-R02) than the MRA model, and half of the calculated parameters also show better performance. At four rules (BMA-R04), all parameters but the bead area are estimated more precisely than the MRA. However, the area estimation shows no clear trend since all three coefficients influence its value.

The T_1 and T_2 toe point locations are estimated with the MRA model with 0.70 and 0.71 mm accuracy. In comparison, the BMA-R02 fuzzy system estimated the points within a 0.85 and 0.75 mm radius around the respective toe point, and with twelve rules of the BMA-R12, they are given within a 0.46 and 0.53 mm radius. Comparing the toe points' estimation errors with the bead width shows that the bead width error is between 60 and 70 percent of the cumulative error of the two toe points.

The evaluation of the contact angle estimation shows that for most cases, the fuzzy systems provide under 5° error, while this value for the MRA is around 7°. If we consider the normalized RMS error on the

Table 7
Comparison of the RMS Error values of validation data between measurements and estimations of the different models.

Model	Profiles	w	A_B	$T_1.X$	$T_1.Y$	$T_2.X$	$T_2.Y$	Φ_1	Φ_2
MRA	934	1.43	2.63	1.40	1.20	1.66	0.98	0.4018	0.4133
BMA-R02	838	1.06	1.56	0.71	0.27	0.69	0.29	0.1452	0.1417
BMA-R03	914	0.99	1.62	0.50	0.31	0.81	0.29	0.0928	0.1256
BMA-R04	891	0.81	1.26	0.59	0.41	0.76	0.39	0.1022	0.1390
BMA-R05	872	0.79	1.26	0.52	0.23	0.68	0.36	0.0888	0.1457
BMA-R06	888	0.79	1.26	0.48	0.29	0.65	0.27	0.0817	0.1024
BMA-R07	925	0.69	1.34	0.57	0.23	0.54	0.34	0.0967	0.1148
BMA-R08	880	0.82	1.38	0.46	0.26	0.69	0.32	0.0930	0.1316
BMA-R09	899	0.70	1.30	0.48	0.28	0.63	0.35	0.0894	0.1103
BMA-R10	858	0.95	1.34	0.69	0.28	0.72	0.34	0.1133	0.1301
BMA-R11	899	0.84	1.29	0.57	0.21	0.61	0.25	0.0998	0.1039
BMA-R12	903	0.78	1.36	0.46	0.16	0.56	0.24	0.0779	0.0862

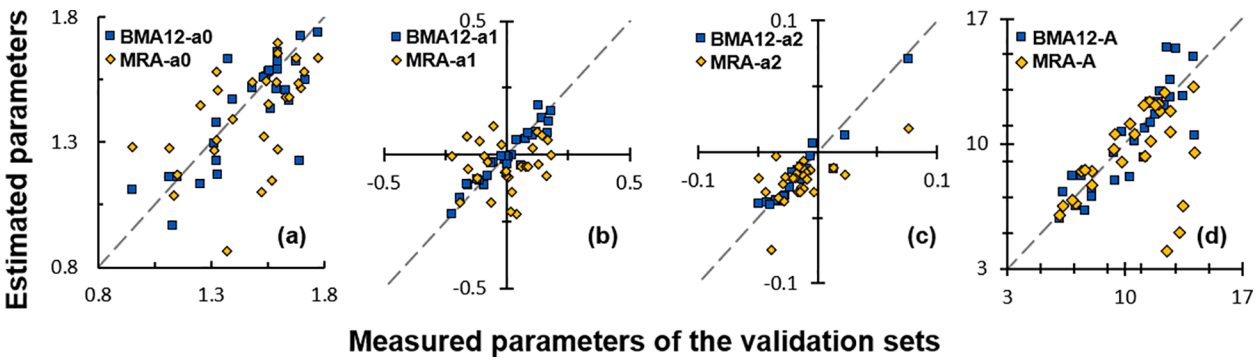

Fig. 8. Fitting plots of the estimated and measured coefficients of the bead shape function and bead area. (a) – (d) comparison of the estimated and measured parameters of the BMA and the MRA models for the validation data set.

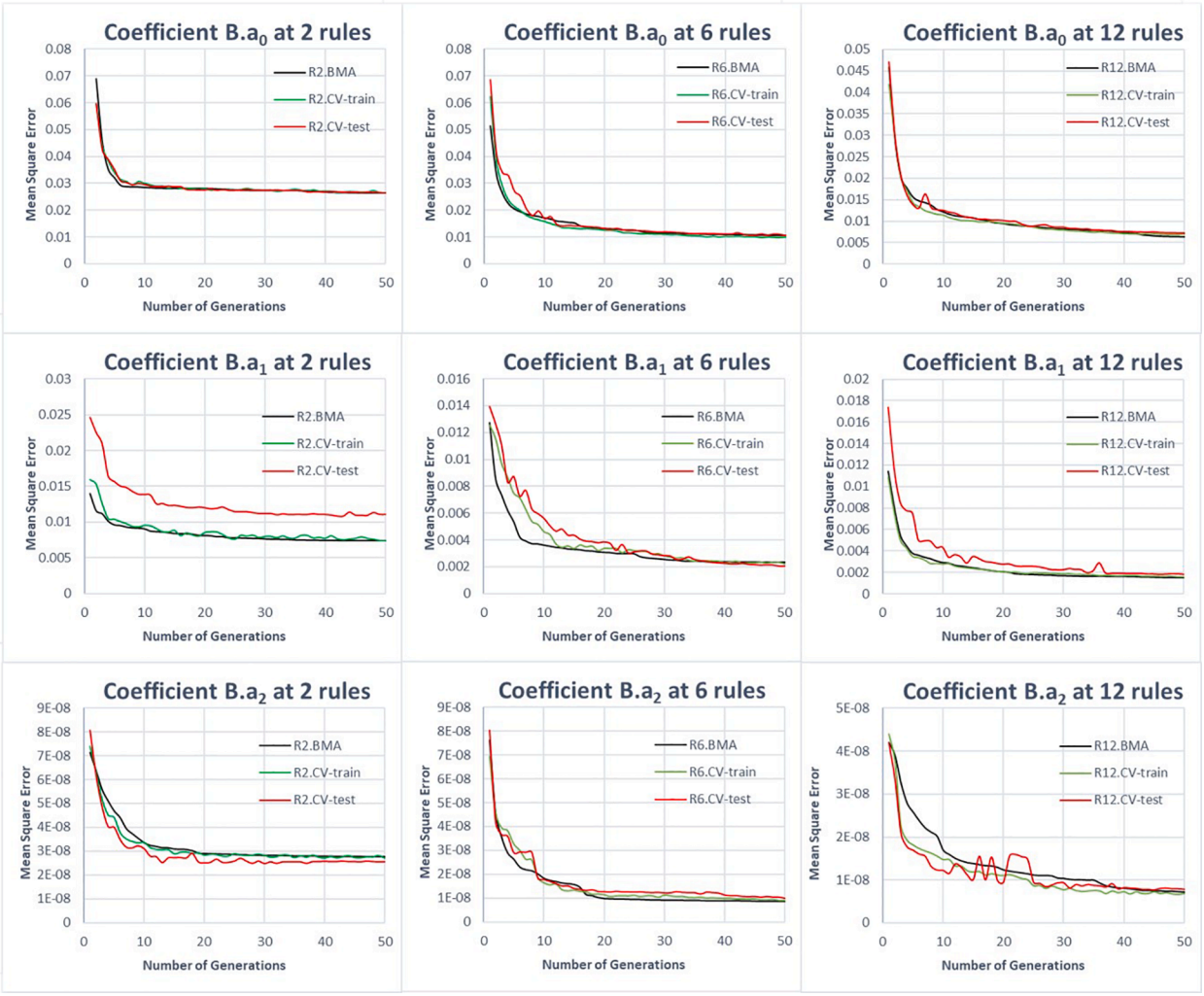

Fig. 9. Illustration of the evolutionary process using BMA with and without cross-validation for $B.a_0, B.a_1, B.a_2$ variables at various number of rules.

ranges of the parameters (Table 1), then we could see that the best BMA-12 model provides the coefficients under three percent precision while the MRA around five percent. The contact angles are estimated with our model with 3.9 and 3.5 percent precision, while the regression model gave twice as big error, 7.4 and 5.8 percent. However, the bead area is estimated fairly close to each other; the MRA gave 7.6, while the BMA model 6.7 percent error on average.

Fig. 7 shows the comparison of the estimated and measured parameters (bead coefficients and bead area) for the best performing BMA-R12 fuzzy system (a-d) and the MRA model (e-h). For the training data, similar fitting can be seen as the results in Table 6 suggests; however, several outlier points can be discovered in (f) compared to (b), and also in (g) compared to (c).

Similar results can be read from the RMSE values of the validation

Table 8
Comparison of the RMS Error values of training data between models developed with and without cross-validation.

(Training)	$B.a_0$				$B.a_1$				$B.a_2$			
	cross-validation		normal BMA		cross-validation		normal BMA		cross-validation		normal BMA	
Model	mean	best	mean	best	mean	best	mean	best	mean	best	mean	best
R02	0.1621	0.1599	0.1628	0.1608	0.0827	0.0798	0.0835	0.0822	0.0164	0.0163	0.0166	0.0165
R03	0.1320	0.1271	0.1327	0.1291	0.0636	0.0621	0.0634	0.0621	0.0122	0.0121	0.0124	0.0120
R04	0.1156	0.1129	0.1139	0.1105	0.0576	0.0572	0.0564	0.0546	0.0108	0.0104	0.0110	0.0110
R05	0.1044	0.1031	0.1073	0.1056	0.0522	0.0514	0.0516	0.0504	0.0101	0.0097	0.0104	0.0102
R06	0.1005	0.0988	0.1015	0.1003	0.0467	0.0458	0.0488	0.0482	0.0095	0.0094	0.0094	0.0093
R07	0.0941	0.0895	0.0960	0.0922	0.0439	0.0431	0.0441	0.0433	0.0098	0.0097	0.0095	0.0093
R08	0.0922	0.0909	0.0887	0.0866	0.0430	0.0421	0.0431	0.0429	0.0091	0.0089	0.0093	0.0091
R09	0.0873	0.0864	0.0908	0.0881	0.0409	0.0404	0.0416	0.0403	0.0089	0.0087	0.0092	0.0091
R10	0.0860	0.0850	0.0852	0.0845	0.0401	0.0386	0.0402	0.0379	0.0089	0.0085	0.0085	0.0078
R11	0.0816	0.0786	0.0819	0.0800	0.0373	0.0354	0.0370	0.0352	0.0085	0.0083	0.0087	0.0087
R12	0.0797	0.0769	0.0790	0.0776	0.0383	0.0373	0.0385	0.0380	0.0084	0.0084	0.0085	0.0083

data set according to Table 7 and the visualized data in Fig. 8. The MRA estimations are outperformed already by the two rule BMA-R02 fuzzy system for all parameters. The proposed model shows the best results with twelve rules except for $B.a_0$ and A_B. The toe points' estimations remained in the same range, maintaining the same ratio with the width error. The contact angles are given with a high error by the MRA (over 23°) and a slight increase for the fuzzy rules, but then the best fuzzy system provided the estimates still with a 5° accuracy. Regarding the Normalized RMS error values, the BMA estimation for $B.a_1$ and $B.a_2$ is still under three percent, while the error of $B.a_0$ increased to 5.2 percent. The MRA model estimations for the coefficients are 8.1, 12.4, and 5.4 percent, respectively. While the magnitude of the error in the case of the BMA-R12 model stays in the same region as was for the training data, the MRA estimations show around 20 percent error in most characteristics and around 40 percent for the Toe point estimation. As a comparison, the toe points by the BMA-R12 model are estimated at 11.7 and 12.3 percent error.

The above analysis can be concluded that the bead geometry deposited on uneven surfaces can be estimated by our proposed model and can be utilized to examine the beads' features.

4.3. Cross-validation

The effect of cross-validation technique is also investigated. In order to realize cross-validation, modifications were applied in how the BMA is executed. The validation dataset is kept unchanged. The training patterns were divided into two subsets: training and testing.

For the testing subsets, tenfold cross-validation was chosen, where at the start of each training process, the training patterns were ordered randomly to one of the ten subsets, creating equal size subsets. Then, in each generation, one of the subsets is selected as a test dataset and the training is performed on the remaining nine subsets as training data. At the end of each generation, the best bacterium is selected according to its performance on the training data, but it is also evaluated on the test subset. Illustration of such evaluation process is shown in Fig. 9, where the original BMA without cross-validation and the BMA with cross-validation can also be seen (in this latter case showing the training and test evolution) for $B.a_0, B.a_1$, and $B.a_2$ variables at a various number of rules.

The training process was repeated three times for each rule number due to the stochastic nature of the process. Each time the training process started, the training patterns were reshuffled. The best results of the three runs and their averages are presented in Table 8 for the training patterns and in Table 9 for the validation patterns for $B.a_0, B.a_1$, and $B.a_2$ variables using BMA with cross-validation and the normal BMA without cross-validation.

Fig. 10 shows, that the results for the validation dataset with or without cross-validation are providing a similar RMSE value. The differences are emphasized in Fig. 11, by calculating the effect of the cross-validation on BMA. The percentage values are given as the difference between the RMSE of the BMA with and without cross-validation, normalized on the corresponding parameter's interpretation interval (see Table 1). The negative values can be translated into decreased error by the cross-validation technique.

From Figs. 9–11 and Tables 8, and 9 it can be seen that there is no significant difference between the two approaches. The fuzzy systems were not overtrained, and the BMA could avoid the local optima and converge to the global optimum with both approaches.

4.4. Bead profile estimation in multi-pass welding

As our method's evaluation has shown in the previous section, the proposed model performed well for the individual weld beads. Therefore, a more comprehensive study is given in the following to evaluate the interaction of the bead shape formation during sequential depositing. During the evaluation process, the measured and estimated bead characteristic features were compared, including all the deposited beads. As a measure, an absolute positioning error is calculated for the T_1 and T_2 points, and a relative error for w, A_B, and the Φ_1, Φ_2 angles. The evaluation is repeated with a different starting position in the groove, given by the starting bead number between zero and twenty, with five bead increments. The process is repeated for multiple cross-sections in the welding groove. The results are given as a summary, including all the 36 generated cross-sections along the weld line with the 5 *mm* steps increment.

The same welding groove was used in the evaluation process, which provided the validation data in the previous step. A welding plan is tabulated in Table B.1, showing the planned WPVs combination and the reference tool center position and orientation for each bead in the groove. Furthermore, the measured location of the bead center is shown. The profile measurements were taken before and after each welding section. The overlapped and aligned measurements are sown in Fig. 12. a. The dimensions of the original workpiece were set to the same as described in Section 3.2. However, during the trials' execution, a small degree of distortion is experienced – as visible on the left groove face, represented by the multiple shifted semi-parallel lines. Still, this shrinkage did not influence the individual beads but played a role while defining the modeling process's fitting goodness.

Due to the experienced material distortion, the model estimates were given in two scenarios: (1) The bead deposition is evaluated utilizing the measured bead profile (Bead Surface – BS case), (2) A constant groove cross-section was chosen with an acceptable deviation in all depth, then the measured bead surfaces are added in the middle, while the groove faces are kept (Constant Groove – CG case).

Table 9
Comparison of the RMS Error values of validation data between models developed with and without cross-validation.

(Validation)	$B.a_0$				$B.a_1$				$B.a_2$			
	cross-validation		normal BMA		cross-validation		normal BMA		cross-validation		normal BMA	
Model	Mean	best	Mean	best	Mean	best	Mean	best	Mean	best	Mean	best
R02	0.1772	0.1519	0.1894	0.1741	0.0650	0.0611	0.0686	0.0649	0.0240	0.0198	0.0194	0.0186
R03	0.1840	0.1828	0.2063	0.1479	0.0709	0.0619	0.0753	0.0594	0.0143	0.0133	0.0147	0.0125
R04	0.1658	0.1419	0.1772	0.1656	0.0774	0.0693	0.0693	0.0524	0.0096	0.0091	0.0166	0.0098
R05	0.2324	0.1587	0.2016	0.1614	0.0649	0.0547	0.0664	0.0656	0.0109	0.0102	0.0125	0.0117
R06	0.1651	0.1298	0.1801	0.1407	0.0864	0.0737	0.0794	0.0555	0.0141	0.0126	0.0122	0.0090
R07	0.1693	0.1410	0.2028	0.1386	0.0688	0.0567	0.0730	0.0574	0.0173	0.0141	0.0155	0.0095
R08	0.1617	0.1535	0.1711	0.1505	0.0720	0.0620	0.0658	0.0608	0.0109	0.0088	0.0216	0.0128
R09	0.1580	0.1367	0.1397	0.1610	0.0620	0.0495	0.0830	0.0787	0.0110	0.0094	0.0128	0.0099
R10	0.1595	0.1393	0.1606	0.1410	0.0748	0.0447	0.0709	0.0583	0.0173	0.0110	0.0120	0.0103
R11	0.1735	0.1342	0.1632	0.1434	0.0732	0.0677	0.0720	0.0554	0.0124	0.0096	0.0117	0.0104
R12	0.1389	0.1216	0.1722	0.1215	0.0610	0.0560	0.0603	0.0451	0.0161	0.0103	0.0104	0.0085

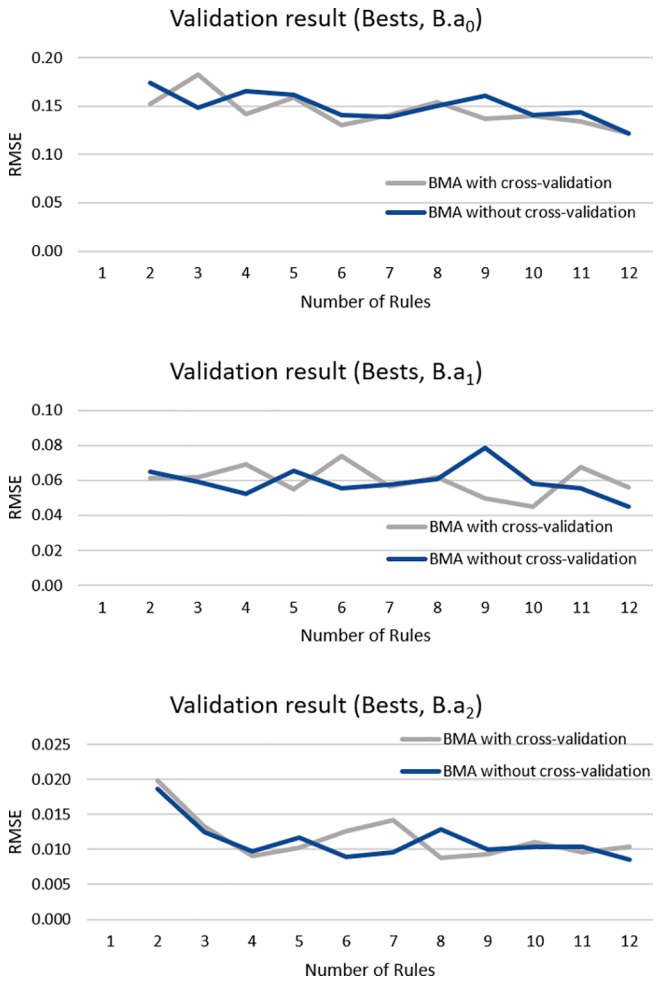

Fig. 10. Trends of RMSE values for $B.a_0, B.a_1, B.a_2$ variables during validation.

We expected that due to the multi-pass welding process's sequential nature, the bead shape estimation deviation would include an accumulating error. The beads in the upper layers would deviate significantly already before the deposition, resulting in higher error in the estimation. The propagation error of the increasing number of layers is handled by starting the deposition by a bead offset, altered from zero to twenty, as shown in Fig. 12 for the CG case and in Fig. 13 for the BS case. In both figures, (a) represents the measurements, and in each sub-images, the black dots show the expected outcome as a reference. The colored lines are the result of the estimation models. According to (b), 31 beads were deposited in the groove, showing the highest difference from the measurements. As the number of deposited beads decreases, the estimations are getting closer to each other since the differences in the segments' description became less significant.

The quantitative evaluation of the bead characteristics in the groove is given in the form of box plots. In both scenarios, the position error of the characteristic points (Fig. 14) and the relative errors (Fig. 15) show a decreasing trend, thus increasing the accuracy of the estimates as less bead deposited and the base metal's segment description is given more precisely to the actual one. The best-fitting is provided when eleven beads were deposited in the upper part of the groove. The typical 10–15 percent error decreases to the 5 percent region, while the position error decreases from the 0.5–1 mm interval to under 0.5 *mm*. This corresponds well with the observed errors calculated for the individual beads. Except for the full groove filling (starting at Bead No. 0), the positioning errors are similar in the two use cases. The BS case shows a larger error due to the higher number of beads in the groove's upper part with a more offset of the groove face. Fitting goodness for the width and area estimations are the opposite – the BS case shows better fitting what can be explained as the detachment of the CG case from the measurements.

The distribution of relative angular errors is shown in Fig. 16. During the complete filling of the groove, the typical error stayed in the 4 –8 percent region, while it remained under five percent in the further cases. This corresponds well with the founding of the analysis of the validation data for the individual beads. The ten percent error was exceeded only in extreme cases. Consequently, we can consider this value as a low error characteristics of the weld bead.

4.5. *Accumulated error of deposition*

The accumulated error of deposition was examined during both groove cross-section. The error value is calculated from the signed difference between the estimated and the measured bead area. The total deposited volume is 315.7 mm^2. In this section, besides the analysis of the pure error accumulation of the estimations, the effect of regular correction is also examined. We reset the error accumulation during the rectification by providing the measured surface after each fifth deposited bead up to the 20*th* bead.

Fig. 17 illustrates the CG case. *CG.estimated* represents the model estimates without any correction. The curve follows a clear trend of slowly accumulating the area estimation error, and by Bead No.30, approximately the area of a medium-sized bead is missing (-11.54 mm^2). This error is a result of many small but constant underestimation of the bead area. As the rectified values show in the *CG*.

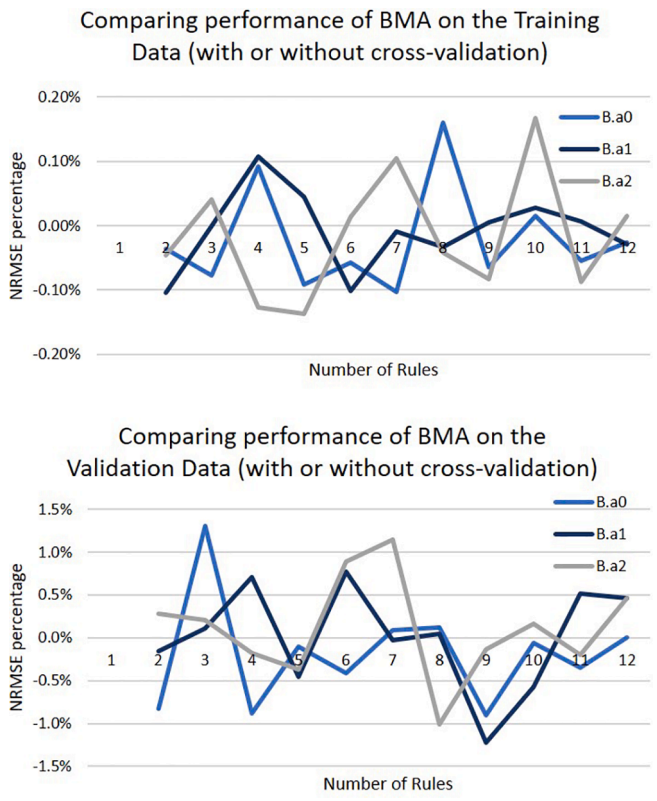

Fig. 11. Comparing the performance of BMA with or without cross-validation for $B.a_0, B.a_1, B.a_2$ variables at the training (above) and validation data (below).

rectified plot, the frequent update of the deposition surfaces keeps the error low, and the final difference is $-1.37\ mm^2$. The case of the measured bead surface deposition is shown in Fig. 18. Compared to the previous case, both the rectified and the uncorrected estimated deposition show a similarly low accumulated error with a slight overestimation of the total deposited area. The *BS.estimated* plot results suggest that the accumulated error is compensated during the deposition; besides, it was initially low for each bead. However, as shown in Fig. 13. (b), the final surface of estimations is significantly different from the measured surfaces, but the covered area is the same due to the groove's shrinkage. This same distortion is the root of the high accumulated error in the CG case. The rectified deposition error of the *BS.rectified* plot supports the model's low estimation error behavior since, in this case, both the estimation area and the estimated surface correlate with the measurements.

4.6. Detecting the welding defect sensitive locations

One of the main advantages of the bead shape function estimation is to gain access to the bead characteristic features, thus, providing an insight to identify locations in the groove where welding defects might occur. The profile measurements suggested such a location, marked in Fig. 13. (a) with a gray arrow. The examination of the macro-etched cross-section of the workpiece verified (Fig. 19) that there is a slag inclusion defect in that location. The root of the error is lack of fusion due to the too narrow and deep gap, which prevented the liquid metal's proper flow, trapping the residue under the melted weld pool. This error should be eliminated immediately after the bead deposition by grinding out defective weld beads in manufacturing. If it is identified only during the workpiece's ultrasonic testing, the defect should be explored open and re-weld, or in the worst case causing scrapping the part.

As Fig. 13. (b) and (c), and Fig. 12. (b) and (c) show, the critical location is identified in the filled grooves with the estimated bead surfaces proving that the proposed model is capable of locating the welding

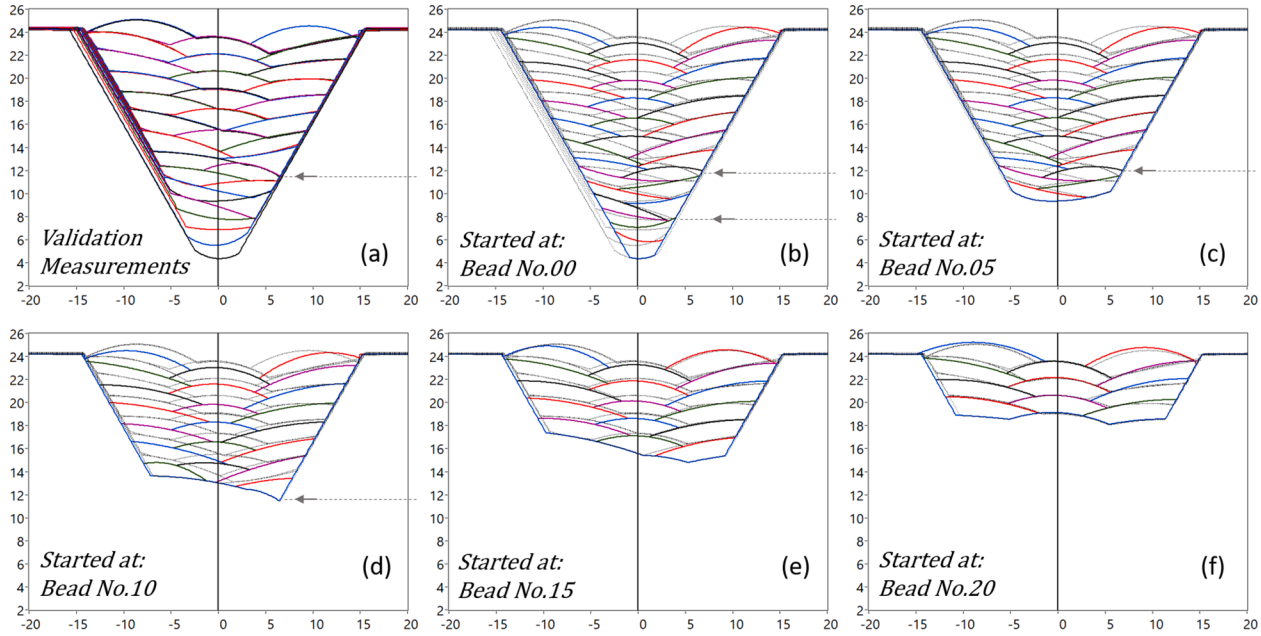

Fig. 12. Plot of (a) the measured bead surfaces and (b)-(f) the estimated bead surfaces in a constant cross-section groove (CG). Gray arrows show the welding defect sensitive locations.

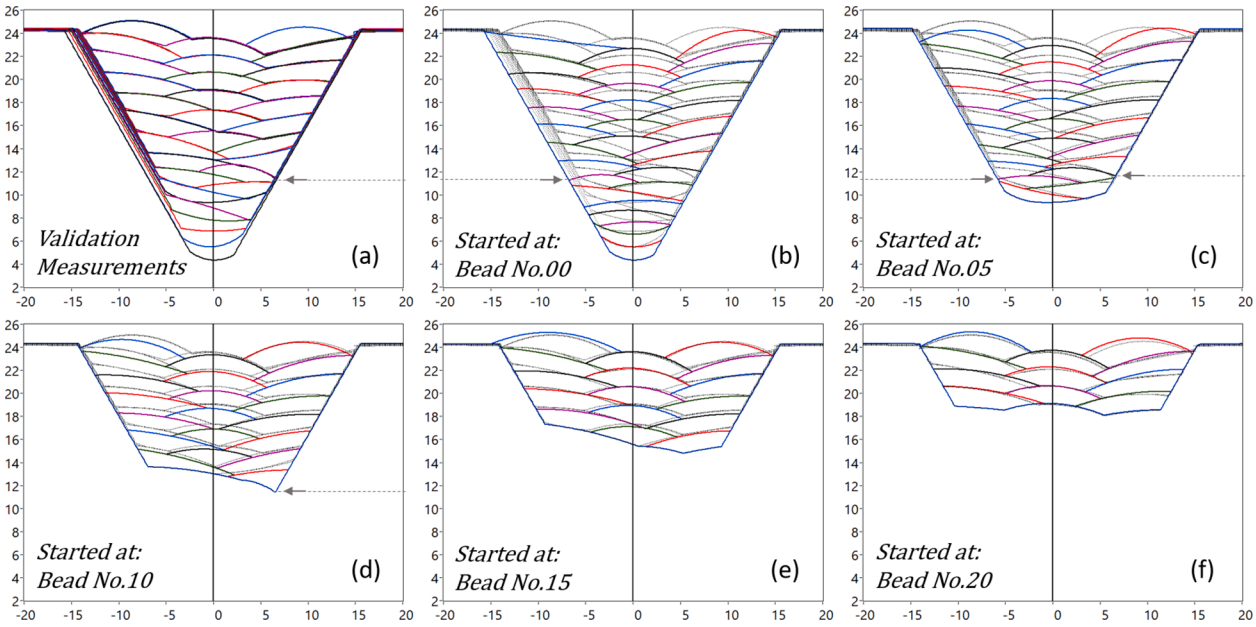

Fig. 13. Plot of (a) the measured bead surfaces and (b)-(f) the estimated bead surfaces in a measured groove surface (BS). Gray arrows show the welding defect sensitive locations.

defect sensitive locations.

5. Conclusion

This paper presented an uneven base metal surface-based modeling method of weld bead profiles and its application in multi-pass welding. The method consists of the weld bead's segmentation and characterization, the base metal from the laser-line scanned profile measurements, and a fuzzy system-based bead profile model.

An empirical model was developed from data of multi-pass and single-pass welding experiments and was validated by comparing the estimated bead profiles with the measurements.

In the first step of the method, the welding data was acquired by processing the workpieces' profile scans to identify the base metal segments and the bead characteristics. The output of the processing is the completely characterized weld bead and the training patterns. The training patterns for machine learning consisted of the welding process variables, the coefficients of the segments function in the weld bead local coordinate system as inputs, and the weld bead surface function's

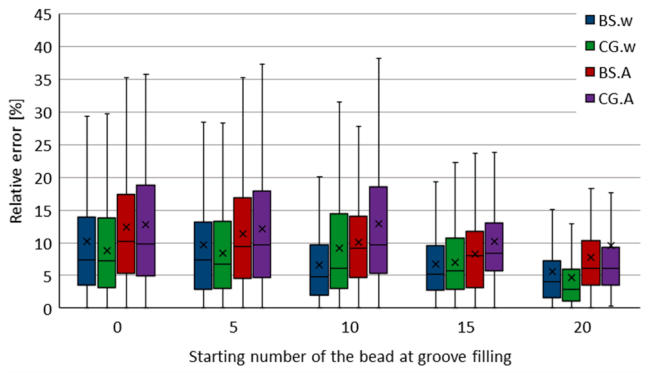

Fig. 15. Relative error of the width and area of the weld beads in case of deposition in a constant cross-section groove and measured bead surface.

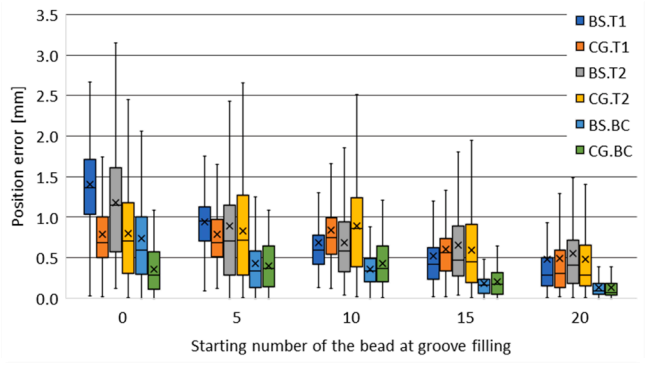

Fig. 14. Position error of the Bead characteristic points T_1, T_2, and Bead center in case of deposition in a constant cross-section groove and measured bead surface.

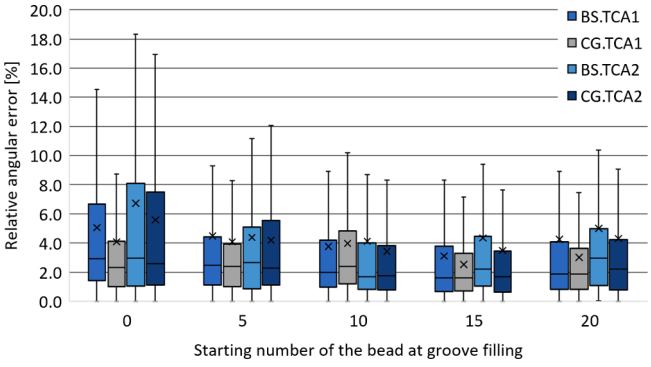

Fig. 16. Relative angular error of the Φ_1 and Φ_2 contact angles of the weld beads in case of deposition in a constant cross-section groove and measured bead surface.

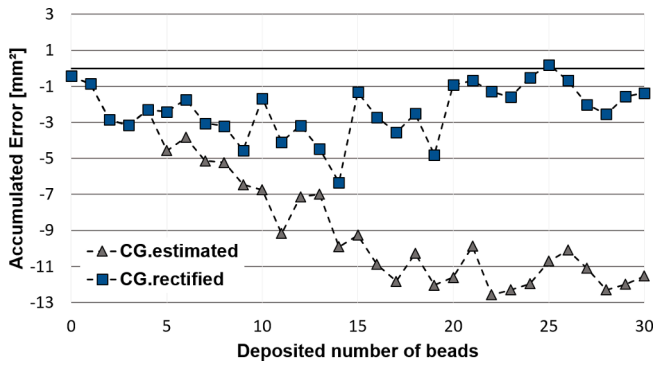

Fig. 17. Accumulated error of the deposited bead area, the estimated bead are compared to the measured total area (Constant Groove cross-section).

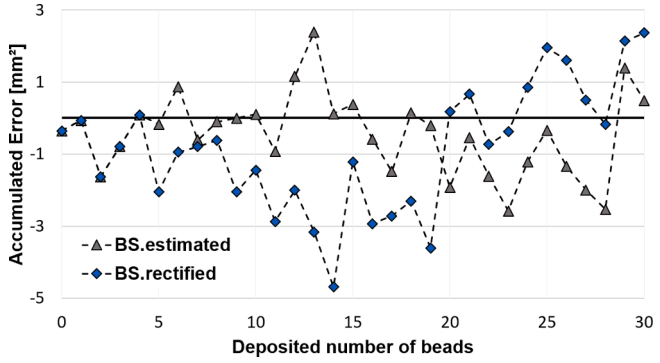

Fig. 18. Accumulated error of the deposited bead area, the estimated bead are compared to the measured total area (Measured Bead Surface cross-section).

coefficients as the outputs.

In the second step, the estimation model was defined as three parallel fuzzy systems. The characteristic points of the trapezoidal membership functions were tuned with the bacterial memetic algorithm during supervised training. The estimated bead profiles showed a good fitting to the measurements validating that the proposed model is suitable for describing the bead profiles in the welding groove when the deposition is made on uneven base metal surfaces.

The results showed that the model achieved a low-error estimation of the calculated bead characteristics. For the individual weld beads, the root square mean error of the estimation was 0.1377,0.0424, and 0.0089 for the coefficients of the bead profile function, which can be translated to under three percent error on the parameter range. While the bead area is estimated at 1.36 mm^2, and the toe points with 0.46 −0.53 mmradius error (corresponding approximately ten percent error on average on the full parameter range), the contact angles are estimated with under 5° or around four percent error.

The developed model was validated during multi-pass welding, where a V-groove was filled with the sequence of estimated weld beads. The results showed a good match with the expected layout, especially during the estimation of the contact angles. The accumulated error of the multi-pass welding was calculated by considering the area of the weld beads. In the test case of a simulated constant groove cross-section, the error increased over time, resulting in a middle-sized bead difference in the end. However, with a simulated measurement of the deposited surface, every fifth weld bead resulted in a one percent error in total. In the other test case, where the measurements were taken as the welding groove's geometry, the accumulated error stayed around below three percent during the deposition with a final error of less than one percent.

Finally, based on the estimation of bead profiles and the contact angles values, the model was able to identify welding defect sensitive locations, matching the defect of the real workpiece.

In our future work, we are intended to explore the proposed model's capability, especially in multi-pass welding in grooves with complex geometry and additive manufacturing, including the welding plan generation feature. The bacterial memetic algorithm can be used in the optimization of bead placement sequences and it also finds the proper welding process variables to produce the required bead. Further directions could be to evaluate deeper integration of cross-validation in our approaches.

CRediT authorship contribution statement

Csongor Márk Horváth: Conceptualization, Data curation, Investigation, Methodology, Project administration, Software, Validation, Visualization, Writing - original draft, Writing - review & editing. **János Botzheim:** Conceptualization, Data curation, Investigation, Methodology, Software, Supervision, Validation, Visualization, Writing - review & editing. **Trygve Thomessen:** Conceptualization, Funding acquisition, Methodology, Project administration, Resources, Supervision, Visualization, Writing - review & editing. **Péter Korondi:** Conceptualization, Funding acquisition, Methodology, Supervision, Visualization, Writing - review & editing.

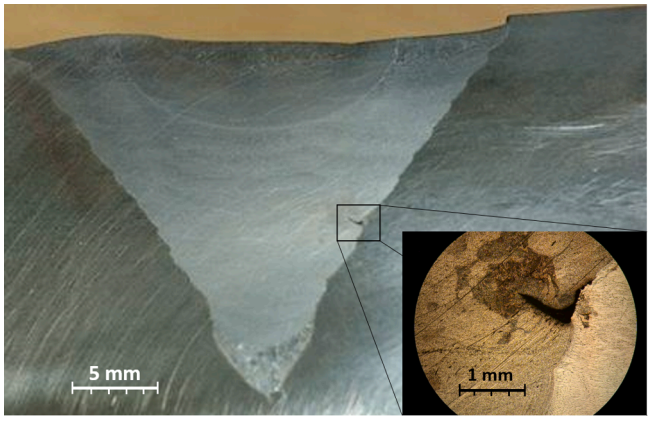

Fig. 19. Cross-section of the workpiece used for validation and the microscopic image of the welding defect (slag inclusion due to lack of fusion).

Declaration of Competing Interest

The authors declare that they have no known competing financial interests or personal relationships that could have appeared to influence the work reported in this paper.

Acknowledgment

PPM Robotics AS and The Norwegian Research Council provided laboratory infrastructure and financial support of this work through the Industrial PhD program (244972/O30) "Virtual presence in remote operation of industrial robot systems", the "CoRoWeld" project (245691) under The User-driven Research based Innovation Program, and the "MultiPass2020" project (293141) under The SkatteFUNN program. The research reported in this paper was supported by the BME NC TKP2020 grant of NKFIH Hungary and by the BME Artificial Intelligence TKP2020 IE grant of NKFIH Hungary (BME IE-MI-FM TKP2020). János Botzheim was supported by the János Bolyai Research Scholarship of the Hungarian Academy of Sciences.

Appendix A. The developed fuzzy systems

The following tables are containing the rules of the developed fuzzy systems.

Table A.1
Mamdani fuzzy system definitions for the $B.a_0$ polynomial function coefficient of the weld bead profile (Fuzzy system settings: AND method: *min*, aggregation method: *max*, defuzzification method: *Center of Sums −COS*).

ID	Current [*A*]	Voltage [*V*]	Torch travel speed [*mm*/*s*]	Wire feed rate [*mm*/*min*]
R01	[177.7 210.4 233.9 297.0]	[9.37 10.17 12.30 16.33]	[2.31 2.63 2.75 3.03]	[401 500 1271 2006]
R02	[173.0 259.0 307.4 310.6]	[11.17 12.55 13.73 15.53]	[2.02 2.26 3.33 3.51]	[708 944 1344 1936]
R03	[144.9 260.5 265.7 302.4]	[10.05 12.23 12.29 12.36]	[2.19 2.40 2.40 2.64]	[799 827 890 1735]
R04	[176.6 273.1 279.1 307.7]	[9.64 10.58 13.61 15.26]	[2.29 2.50 2.66 3.02]	[425 490 1558 1665]
R05	[159.2 218.7 272.3 306.6]	[9.48 11.33 12.03 13.06]	[1.56 2.56 2.67 3.36]	[551 737 1065 1862]
R06	[214.7 230.0 273.1 300.1]	[10.76 11.50 12.60 13.34]	[2.03 2.04 2.64 2.65]	[1122 1379 2009 2166]
R07	[177.0 229.0 238.9 286.7]	[9.16 12.29 15.01 16.36]	[1.56 1.70 2.54 3.57]	[762 1066 1508 2138]
R08	[175.1 201.8 223.7 241.6]	[11.14 12.12 15.48 16.00]	[1.63 2.97 3.21 3.56]	[472 548 763 1576]
R09	[174.9 186.5 241.0 257.6]	[9.70 9.88 10.67 16.58]	[1.81 2.27 2.31 2.90]	[971 1744 2059 2074]
R10	[150.0 193.4 241.5 268.1]	[9.19 10.35 15.96 16.46]	[1.58 2.16 2.70 2.70]	[825 939 1508 2256]
R11	[171.8 193.6 234.0 282.6]	[9.68 10.00 12.86 15.68]	[1.90 1.99 2.04 3.25]	[1444 1528 1530 1921]
R12	[214.5 215.9 250.0 265.7]	[9.70 11.83 13.80 16.16]	[2.49 3.11 3.19 3.27]	[1253 1271 1811 2250]
ID	Segment-1.a_0 [-]	Segment-1.a_1 [-]	Segment-1.a_2 [-]	Segment-2.a_0 [-]
R01	[-9.0163 0.9872 2.3422 2.6423]	[-1.7428 0.2806 0.4087 0.4730]	[-0.1779 -0.0107 0.0916 0.1398]	[-0.1855 -0.0951 0.0564 0.1119]
R02	[-7.8952 -6.1493 -4.8619 -2.9335]	[-1.9676 -1.5674 -0.4679 0.1362]	[-0.1787 -0.1749 -0.0065 0.0528]	[-0.1798 -0.0301 -0.0184 0.0372]
R03	[-2.9248 -1.8972 -0.9204 2.0817]	[-1.6684 -0.4040 -0.1605 -0.0023]	[-0.1170 -0.0218 0.1098 0.1399]	[-0.1724 -0.1460 -0.0736 0.1186]
R04	[-8.1917 -7.0434 -4.1666 0.1889]	[-1.5597 -0.5367 -0.1813 0.0145]	[-0.1042 -0.0495 0.0603 0.1523]	[-0.0772 0.0006 0.0149 0.0469]
R05	[-9.6603 -9.4961 -0.0244 0.9633]	[-1.6070 0.1547 0.2222 0.3922]	[-0.0946 0.0256 0.0395 0.1945]	[-0.1972 -0.1012 -0.0198 0.0818]
R06	[-5.4894 -2.3722 -1.2329 -0.5564]	[-1.2058 -1.2044 -0.1673 0.2414]	[-0.0933 -0.0291 0.0170 0.0392]	[-0.1847 -0.0350 0.0339 0.1311]
R07	[-8.5205 -3.8625 1.4569 2.1417]	[-1.4044 -0.8143 -0.6996 0.0835]	[-0.1401 -0.1192 0.0061 0.0895]	[-0.1680 -0.0400 0.0672 0.1169]
R08	[-5.6877 -4.1035 -2.2077 -1.8841]	[-1.9324 -1.4382 -1.3531 -0.2484]	[-0.0998 -0.0602 0.0077 0.1946]	[-0.1275 0.0262 0.0293 0.0491]
R09	[-7.6782 -0.1865 0.4213 0.9988]	[-1.7258 -1.6893 -0.4246 0.2523]	[-0.0556 -0.0290 -0.0146 0.0837]	[-0.1375 -0.1214 -0.0611 0.0567]
R10	[-8.1149 -6.7038 -1.9597 1.6364]	[-1.5520 -0.7798 -0.4498 0.3874]	[-0.1586 0.0006 0.0008 0.0585]	[-0.0449 0.0039 0.0249 0.1185]
R11	[-8.8082 -1.0270 -1.0207 1.2584]	[-1.9882 -1.5161 -0.7513 0.2304]	[-0.1931 -0.1628 -0.1225 0.0227]	[-0.1261 -0.0372 0.0473 0.0727]
R12	[-3.6880 -0.7400 1.1617 1.6442]	[-1.4152 -1.2562 -0.9937 0.4147]	[-0.0610 -0.0366 0.0019 0.1049]	[-0.1567 -0.0145 0.0515 0.1200]
ID	Segment-2.a_1 [-]	Segment-2.a_2 [-]	Segment-3.a_0 [-]	Segment-3.a_1 [-]
R01	[-0.9756 -0.2622 0.5783 0.7314]	[-0.1757 -0.1700 0.1067 0.3605]	[-6.6747 -4.1009 1.1217 2.6907]	[-0.4244 -0.2714 1.9178 2.0199]
R02	[-1.2894 -0.1676 0.0692 0.2311]	[-0.1375 -0.1335 0.3440 0.5599]	[-6.2237 -5.2007 -1.1479 -0.7217]	[-0.4097 0.0938 1.2438 1.7475]
R03	[-0.6734 -0.5688 -0.2544 0.8306]	[-0.4465 -0.1933 0.2238 0.2334]	[-0.5093 0.3105 0.5544 2.6813]	[-0.1410 0.5417 0.8835 1.6744]
R04	[-0.9266 -0.0752 0.6808 1.3827]	[0.0267 0.0315 0.5564 0.6072]	[-7.9384 -6.5539 -6.2052 0.5206]	[0.0141 0.4671 0.9597 1.4981]
R05	[-0.7244 -0.4499 -0.2170 0.9913]	[-0.4227 -0.2633 0.0142 0.5717]	[-4.4337 -2.7435 0.0437 2.2119]	[-0.4155 -0.3990 -0.3609 1.5838]
R06	[-1.2327 -1.1929 0.0756 0.2573]	[-0.4271 -0.4063 0.1012 0.5424]	[-5.6654 -2.4828 -1.1740 1.1692]	[-0.4494 0.1554 1.1724 1.2135]
R07	[-1.3616 -1.2425 1.3987 1.5589]	[-0.1864 -0.1331 0.1519 0.5499]	[-2.2505 -0.0240 1.2115 2.7334]	[0.4051 0.7320 0.7922 2.0390]
R08	[-1.3715 -1.1500 1.1025 1.4132]	[-0.3615 -0.2743 0.0773 0.1876]	[-6.0684 -4.0760 2.1144 2.5004]	[-0.4885 -0.4069 1.3781 1.6556]
R09	[-0.9417 -0.7745 -0.4048 0.6829]	[-0.4337 -0.2821 -0.2592 0.6090]	[-4.3911 -0.3998 0.3504 1.4935]	[-0.2942 -0.2204 1.1436 1.8560]
R10	[-0.4353 0.2277 0.2328 0.3589]	[-0.4166 -0.0705 0.3109 0.3363]	[-8.5701 -5.6454 -3.7169 2.4415]	[-0.0698 0.3791 0.9464 1.7202]
R11	[-1.2941 0.8353 0.9798 1.2042]	[-0.1949 -0.1021 0.2876 0.5425]	[-6.2965 -1.5759 -1.4718 2.2909]	[-0.1211 0.6300 1.1697 1.5098]
R12	[-1.0789 0.6278 0.9942 1.3378]	[-0.2512 -0.1757 -0.1132 -0.0437]	[-8.5257 -3.9127 0.5298 1.4944]	[0.8530 0.8834 1.6460 1.7391]
ID	Segment-3.a_2 [-]	Output: Bead.a_0 [-]		
R01	[-0.0977 -0.0827 0.0042 0.1091]	[0.4561 0.4571 0.8769 0.9705]		
R02	[-0.0973 -0.0188 -0.0071 0.0414]	[0.4562 0.4565 1.1109 1.5912]		
R03	[-0.1681 0.0434 0.0446 0.0654]	[2.1315 3.0217 3.2921 3.3221]		
R04	[-0.1960 -0.1038 0.0712 0.1822]	[1.8963 2.8169 3.2135 3.2137]		
R05	[-0.2025 -0.1066 -0.0435 0.1787]	[0.4561 0.4561 0.5617 2.0691]		
R06	[-0.1749 -0.0599 0.0130 0.1093]	[0.4561 0.4600 1.4254 1.4670]		
R07	[-0.1718 -0.0373 0.1796 0.1797]	[2.6510 3.1196 3.5103 3.6040]		
R08	[-0.1300 -0.0017 0.0987 0.1581]	[0.4574 0.4765 0.5936 1.8074]		
R09	[-0.1744 0.0417 0.1494 0.1647]	[1.7719 1.8857 2.6774 2.8179]		
R10	[-0.0913 -0.0150 -0.0108 0.0230]	[0.5023 0.5475 1.2611 2.5117]		
R11	[-0.0814 -0.0278 0.0209 0.0326]	[2.4723 2.7388 2.7391 3.1247]		
R12	[0.0459 0.0786 0.1020 0.1459]	[1.0512 3.2276 3.4615 3.7675]		

Table A.2
Mamdani fuzzy system definitions for the $B.a_1$ polynomial function coefficient of the weld bead profile (Fuzzy system settings: AND method: *min*, aggregation method: *max*, defuzzification method: *Center of Sums −COS*).

ID	Current [*A*]	Voltage [*V*]	Torch travel speed [*mm*/*s*]	Wire feed rate [*mm*/*min*]
R01	[187.9 244.8 261.7 283.8]	[9.19 12.93 13.89 14.78]	[1.99 2.09 2.16 3.05]	[712 789 1586 1893]
R02	[171.8 268.9 299.5 310.2]	[12.32 14.16 15.83 15.94]	[1.81 2.47 3.33 3.45]	[470 1651 1869 1911]
R03	[164.2 180.7 188.0 288.1]	[9.67 10.18 10.90 13.00]	[1.83 1.94 2.45 3.29]	[623 692 733 1430]
R04	[174.2 252.2 282.8 294.8]	[10.10 10.73 11.50 15.46]	[2.13 2.83 2.94 3.43]	[558 686 706 1883]
R05	[184.0 219.7 221.1 268.8]	[9.85 9.93 13.48 16.53]	[2.00 2.20 2.20 3.03]	[905 1022 1655 1849]
R06	[161.0 180.7 202.4 307.8]	[9.87 12.75 13.59 14.39]	[1.90 2.59 2.90 3.01]	[605 1146 1344 1463]
R07	[159.7 163.0 173.2 245.0]	[9.13 11.82 13.89 14.78]	[1.90 2.21 2.26 3.29]	[698 744 1785 2150]
R08	[154.7 162.8 214.8 278.1]	[9.17 12.15 13.08 14.73]	[1.90 2.84 2.93 2.98]	[656 721 848 1878]
R09	[173.5 213.1 216.4 225.5]	[11.99 12.06 15.77 15.86]	[1.84 1.93 2.21 3.07]	[775 913 2113 2277]
R10	[168.5 247.0 256.1 256.8]	[10.90 12.26 15.53 16.46]	[1.84 2.07 2.55 3.09]	[634 1088 1129 1329]
R11	[164.9 197.2 243.1 252.5]	[10.27 10.67 14.04 16.16]	[1.59 1.59 2.14 2.89]	[460 547 1149 1913]
R12	[152.9 177.2 179.9 292.2]	[11.49 12.17 12.39 16.37]	[2.10 2.90 3.02 3.46]	[613 661 1746 1900]
ID	Segment-1.a_0 [-]	Segment-1.a_1 [-]	Segment-1.a_2 [-]	Segment-2.a_0 [-]
R01	[-5.8622 -2.8972 -2.7971 2.4865]	[-2.0515 -1.3389 -1.1469 0.2519]	[-0.1532 0.0499 0.1016 0.1938]	[-0.2108 -0.0608 -0.0124 0.0771]
R02	[-7.5906 1.3370 2.5319 2.7100]	[-1.9758 -1.7887 -0.2620 0.4398]	[-0.0129 0.0540 0.0633 0.0888]	[-0.2180 -0.1666 0.0007 0.0162]
R03	[-8.8579 -4.8905 -3.4487 0.8289]	[-1.4406 -1.3229 -0.5135 0.3747]	[-0.1746 -0.0872 -0.0616 0.1232]	[-0.2004 -0.1249 -0.0552 0.0272]
R04	[-7.9444 -5.8706 -1.7662 0.9235]	[-1.2457 -0.6754 0.2855 0.3388]	[-0.1372 -0.0621 -0.0563 0.1763]	[-0.1552 -0.0576 -0.0574 0.1169]
R05	[-7.0021 -6.3005 -6.1894 0.9468]	[-1.4531 -1.2579 0.0067 0.1333]	[-0.1499 -0.0869 -0.0712 0.0571]	[-0.2171 -0.2159 -0.0691 0.0868]
R06	[-9.4796 -2.0253 -0.5267 0.2288]	[-1.4437 -1.2680 0.1121 0.2539]	[-0.1890 0.0669 0.0697 0.0950]	[-0.1250 0.0603 0.1071 0.1239]
R07	[-7.8384 -7.3173 -3.7322 -1.5746]	[-1.6003 -0.9935 -0.9911 -0.5634]	[-0.0822 0.0957 0.1016 0.1641]	[-0.2108 -0.1499 0.0467 0.0748]
R08	[-8.2177 -4.9113 -3.7259 -1.4310]	[-1.6944 -1.5734 -0.5088 -0.2922]	[-0.1827 -0.0524 0.1059 0.1866]	[-0.2118 -0.1821 0.0820 0.1291]
R09	[-3.7143 -0.5490 -0.5466 -0.1994]	[-2.0508 -1.9931 -1.3796 -0.3955]	[-0.0887 0.0167 0.0174 0.0513]	[-0.1107 -0.0310 -0.0206 0.1138]
R10	[-6.0317 -5.2826 0.1788 0.6305]	[-2.0093 -1.9701 -0.6512 0.0219]	[-0.0891 0.0738 0.1725 0.1917]	[-0.1938 -0.1238 0.0279 0.0739]
R11	[-8.0176 -3.2134 -2.6361 -2.5892]	[-1.9711 -1.4898 -1.4174 -1.0171]	[-0.1977 -0.1689 0.0820 0.0958]	[-0.0887 0.0239 0.0333 0.0410]
R12	[-5.5857 -2.9890 -2.9666 0.7672]	[-2.0370 -1.9510 -0.6238 -0.1751]	[-0.0697 0.0041 0.0929 0.1819]	[-0.1256 -0.0924 0.1082 0.1217]
ID	Segment-2.a_1 [-]	Segment-2.a_2 [-]	Segment-3.a_0 [-]	Segment-3.a_1 [-]
R01	[-0.6262 -0.4963 -0.4671 1.1033]	[-0.4326 -0.0109 0.0555 0.5425]	[-5.7375 -5.2226 -0.1276 1.1567]	[-0.1781 0.3109 0.7603 1.5447]
R02	[-0.7190 0.7786 1.3246 1.5174]	[-0.3782 -0.3024 -0.2071 -0.1608]	[-9.4780 -6.9101 -5.6343 -3.5537]	[-0.4902 0.1962 0.4580 1.5939]
R03	[-0.2693 0.8948 1.3525 1.4827]	[-0.3911 -0.2857 0.3072 0.5549]	[-7.7754 -1.6498 0.1562 1.7843]	[0.1825 1.5395 1.5739 1.5882]
R04	[-0.5818 -0.4233 1.3374 1.4301]	[-0.3364 -0.2980 -0.1349 0.1702]	[-5.1662 -2.8241 -1.1139 0.7283]	[0.0291 1.5079 1.7900 1.8352]
R05	[-0.2594 0.0763 1.3718 1.4814]	[-0.3205 -0.0781 0.3329 0.3994]	[-9.6831 -7.6627 -3.4002 2.1406]	[-0.2783 0.1640 1.1566 1.6597]
R06	[-1.2465 -1.0536 -0.2481 0.4839]	[-0.1421 0.1087 0.2134 0.4339]	[-8.2576 -6.6140 -2.4465 -1.9551]	[-0.1771 0.6985 1.3216 1.5162]
R07	[-1.2790 0.2177 0.9037 1.5458]	[-0.2099 0.0278 0.1565 0.6197]	[-7.2805 2.2658 2.4639 2.7178]	[-0.0884 0.3845 0.8111 1.8037]
R08	[-1.0337 -0.0153 0.4817 1.5036]	[-0.3272 -0.2467 0.4117 0.4845]	[-8.2185 -8.1380 0.3422 0.6248]	[-0.2055 -0.1756 1.3993 1.4448]
R09	[-1.1949 0.4299 0.9357 1.5278]	[-0.3069 -0.2979 -0.2774 0.4559]	[-9.7425 -8.2847 -0.7519 1.4794]	[-0.4237 0.8056 1.1737 1.4830]
R10	[-1.5030 -1.1086 -0.9477 0.8226]	[-0.4433 -0.1547 -0.1516 0.5450]	[-9.8226 -9.2775 -3.3123 -1.4074]	[-0.0342 0.7926 0.9139 1.4816]
R11	[-1.4327 -0.7518 0.4817 0.5577]	[-0.2222 -0.1824 -0.0703 0.5315]	[-4.2259 -0.4584 0.1194 1.7442]	[-0.1717 0.4248 1.9005 2.0160]
R12	[-0.8539 -0.5682 -0.1558 1.0811]	[-0.3857 -0.3654 0.1582 0.1787]	[-3.0209 -2.6642 -0.0523 0.8471]	[-0.4641 -0.2627 0.0802 0.6869]
ID	Segment-3.a_2 [-]	Output: Bead.a_0 [-]		
R01	[-0.1688 -0.0892 0.1190 0.1432]	[-1.2827 -1.1323 -0.4826 1.3546]		
R02	[0.0315 0.0563 0.1157 0.1283]	[-0.0501 0.0107 0.9724 1.1102]		
R03	[-0.1856 -0.1111 0.0502 0.1081]	[0.6989 0.9611 1.3459 1.3540]		
R04	[-0.0839 0.0533 0.0537 0.0627]	[-0.6329 0.7745 1.2174 1.2303]		
R05	[-0.0410 0.0016 0.0741 0.1445]	[-1.3157 1.1513 1.1949 1.2631]		
R06	[-0.1842 -0.1604 -0.0891 0.1998]	[-1.2157 -1.1409 0.3851 1.3041]		
R07	[-0.2038 0.0939 0.1388 0.2008]	[-1.3049 -0.7196 1.2554 1.3316]		
R08	[0.0006 0.0357 0.1601 0.1928]	[-1.4222 -0.8067 1.0234 1.1821]		
R09	[-0.0345 -0.0251 0.0043 0.1769]	[-1.3750 -1.3679 -0.8537 1.0049]		
R10	[-0.0901 -0.0871 0.0118 0.0439]	[-1.3775 -1.3772 -1.3744 -0.2538]		
R11	[-0.2027 -0.1501 -0.0150 -0.0130]	[-1.4172 -0.7736 1.0619 1.0643]		
R12	[-0.0602 0.0229 0.1623 0.1773]	[-1.3200 -1.3194 -1.2002 1.2294]		

Table A.3
Mamdani fuzzy system definitions for the $B.a_2$ polynomial function coefficient of the weld bead profile (Fuzzy system settings: AND method: *min*, aggregation method: *max*, defuzzification method: *Center of Sums −COS*).

ID	Current [A]	Voltage [V]	Torch travel speed [mm/s]	Wire feed rate [mm/min]
R01	[150.2 167.8 226.4 279.9]	[11.34 12.00 12.08 13.70]	[1.85 2.43 3.23 3.29]	[911 1653 1979 2182]
R02	[170.5 207.6 241.3 245.8]	[9.16 11.07 12.52 16.30]	[1.77 2.16 2.22 2.32]	[916 1114 1123 1139]
R03	[151.5 197.8 264.7 299.8]	[11.13 11.55 12.11 12.31]	[1.56 1.64 1.99 3.57]	[421 562 574 1230]
R04	[179.7 205.2 206.9 207.7]	[9.45 10.90 15.38 15.58]	[1.71 1.72 2.74 2.94]	[714 941 1042 1144]
R05	[151.1 172.8 277.7 301.5]	[10.04 11.35 13.27 15.32]	[2.16 3.22 3.31 3.53]	[1431 1567 1620 1913]
R06	[178.1 210.5 258.7 273.5]	[10.76 12.23 12.44 14.11]	[1.84 2.16 2.61 3.01]	[532 1341 1383 2063]
R07	[186.6 190.5 263.1 298.3]	[9.29 9.45 12.90 15.63]	[2.50 2.52 3.20 3.39]	[518 547 1258 1634]
R08	[179.4 196.0 291.9 310.4]	[10.29 10.52 13.15 13.93]	[1.84 1.84 1.88 3.01]	[485 602 1540 1868]
R09	[192.3 203.6 301.9 303.6]	[9.90 10.12 10.16 12.30]	[1.84 2.15 2.88 3.39]	[529 551 642 1347]
R10	[146.2 164.9 193.2 201.1]	[11.88 12.44 12.51 12.76]	[1.88 1.92 2.00 3.13]	[455 481 1542 1981]
R11	[187.1 233.3 235.1 296.2]	[9.49 9.65 11.07 13.22]	[1.90 2.19 2.79 3.25]	[748 752 1574 1781]
R12	[177.9 185.4 263.9 304.1]	[10.16 10.40 11.75 16.26]	[2.37 2.77 3.10 3.47]	[992 1291 2000 2269]
ID	Segment-1.a_0 [-]	Segment-1.a_1 [-]	Segment-1.a_2 [-]	Segment-2.a_0 [-]
R01	[-8.7291 -4.0657 0.3994 1.5906]	[-1.3950 -0.7099 0.3664 0.4519]	[-0.0953 0.0018 0.0480 0.0677]	[-0.1282 -0.0152 -0.0046 0.0913]
R02	[-10.0103 -6.4535 -2.6680 2.3204]	[-1.9065 -1.3372 -1.1642 0.1531]	[-0.1386 0.0601 0.1553 0.2033]	[-0.1870 -0.1725 -0.0045 0.0958]
R03	[-8.0854 -6.7511 -4.7392 0.3061]	[-1.5095 -1.2007 -0.9176 0.4332]	[-0.0286 -0.0036 0.0060 0.0519]	[-0.1789 -0.0149 0.0543 0.0566]
R04	[-7.3475 -6.7077 -6.7065 -3.9485]	[-1.4671 -0.9162 -0.2202 -0.2043]	[-0.0223 0.0918 0.1220 0.1938]	[-0.1816 -0.1484 0.0373 0.0580]
R05	[-10.0597 -7.9424 -1.9385 -1.5795]	[-1.8847 -1.6472 -0.2765 0.4953]	[-0.1938 -0.1626 -0.1577 -0.1108]	[-0.1824 -0.1366 -0.1109 -0.1085]
R06	[-6.2514 -0.1165 0.4951 2.2950]	[-1.8448 -1.1279 -0.3255 0.3511]	[-0.1730 -0.0031 0.1471 0.1912]	[-0.1880 0.0244 0.0867 0.1212]
R07	[-5.1620 -4.2983 0.1016 1.4353]	[-1.5771 -1.5332 -0.2794 0.0085]	[-0.0972 -0.0867 0.0017 0.1067]	[-0.0963 -0.0872 0.1146 0.1288]
R08	[-9.3204 -4.2948 -0.3922 0.0017]	[-1.7862 -1.2253 -1.0395 -0.1885]	[-0.0862 -0.0496 -0.0439 0.1095]	[-0.1198 -0.1191 -0.1087 0.0542]
R09	[-8.1099 -7.6049 -7.1880 -0.1435]	[-1.4429 -1.3992 -0.5704 0.4023]	[-0.0239 0.1291 0.1505 0.1713]	[-0.1309 -0.0088 -0.0044 0.0430]
R10	[-6.1882 -0.5275 1.9689 2.5674]	[-2.0493 -1.5032 -1.4543 -0.6314]	[-0.1675 -0.0645 0.0207 0.2012]	[-0.2026 -0.0638 -0.0515 0.1051]
R11	[-8.6051 -5.8701 -0.7933 0.7541]	[-1.5496 -0.8912 0.0460 0.2428]	[-0.0671 -0.0581 0.0680 0.0901]	[-0.1101 -0.0628 -0.0238 0.1229]
R12	[-2.9871 -2.3055 -1.0648 -0.5324]	[-1.7748 -1.0454 -0.6879 0.0554]	[-0.1975 -0.0339 0.0692 0.1587]	[-0.1854 -0.0440 0.0477 0.1349]
ID	Segment-2.a_1 [-]	Segment-2.a_2 [-]	Segment-3.a_0 [-]	Segment-3.a_1 [-]
R01	[-0.8904 0.0427 0.0748 0.8877]	[-0.1547 -0.0390 0.1942 0.4183]	[-8.4967 -6.1152 0.0842 1.6189]	[-0.1441 -0.1165 -0.0079 1.7796]
R02	[-0.8852 -0.8400 -0.7573 0.4734]	[-0.4215 -0.3949 -0.0319 -0.0046]	[-5.7698 -1.0308 -0.8404 1.9988]	[-0.2262 0.2382 0.4848 1.3663]
R03	[-0.7353 -0.2839 1.1161 1.1727]	[-0.1796 -0.1197 0.1119 0.3131]	[-8.3675 -7.8209 1.6490 2.5738]	[-0.4504 -0.4349 -0.3173 -0.0169]
R04	[0.0542 0.7110 0.8833 1.1025]	[-0.4162 -0.3135 0.5550 0.5893]	[-0.4464 1.0314 1.2661 1.6721]	[-0.4772 -0.3293 -0.3188 0.3174]
R05	[-0.3332 -0.0677 -0.0111 1.4940]	[-0.3177 0.1461 0.1552 0.5184]	[-5.1092 -4.7012 -4.6259 1.4303]	[-0.4781 -0.1429 -0.0660 0.6304]
R06	[-1.5123 -1.4762 1.0940 1.2068]	[-0.2009 -0.0633 0.0155 0.1051]	[-6.0670 -1.9054 2.2205 2.2446]	[-0.3992 0.4170 0.8155 1.7564]
R07	[-0.5928 -0.5429 1.3379 1.5364]	[-0.1035 -0.0427 0.1291 0.1827]	[-5.0606 -2.6745 0.4644 0.9948]	[-0.3778 0.1882 1.6414 1.8456]
R08	[-1.4954 -1.2795 0.2037 0.7423]	[-0.1624 0.1421 0.4144 0.5146]	[-7.5596 -1.6419 -1.2899 1.2050]	[-0.1822 1.8065 1.8189 1.9878]
R09	[0.1314 0.4766 1.0338 1.3755]	[-0.2751 -0.1524 0.1425 0.2648]	[-5.7656 -4.6515 -2.7881 0.8978]	[0.4550 0.5045 0.9996 1.5993]
R10	[-1.4881 -0.1572 0.1055 1.4915]	[-0.4339 -0.3118 -0.2749 0.0570]	[-5.9051 -0.9436 -0.6293 -0.2015]	[1.1533 1.2586 1.7961 1.8618]
R11	[-1.1548 -0.7712 -0.7149 0.9812]	[-0.1680 -0.0802 0.2805 0.4449]	[-5.9310 0.8670 2.6987 2.7084]	[0.6627 1.6515 1.8628 1.9483]
R12	[-1.0176 -0.7365 -0.6541 -0.0972]	[-0.2158 -0.1189 0.3131 0.4062]	[-9.0642 -5.6870 -5.2877 -0.8029]	[-0.3311 -0.1501 0.6366 0.7070]
ID	Segment-3.a_2 [-]	Output: Bead.a_0 [-]		
R01	[-0.1088 -0.0992 0.0362 0.1806]	[-0.1772 -0.1695 -0.0111 0.0610]		
R02	[-0.1229 -0.0834 -0.0504 0.0303]	[-0.3376 -0.3091 -0.2873 0.0846]		
R03	[-0.1848 -0.1255 -0.0414 0.0154]	[-0.3306 -0.1777 -0.0965 0.0543]		
R04	[-0.1454 -0.0906 0.0296 0.1316]	[-0.3387 -0.3347 -0.3237 0.0881]		
R05	[-0.1316 -0.1108 -0.0789 -0.0457]	[-0.1626 -0.0771 -0.0387 0.0505]		
R06	[-0.1591 -0.0124 0.1160 0.1670]	[-0.1872 0.0902 0.0931 0.0931]		
R07	[-0.0795 -0.0403 0.0155 0.1417]	[0.0277 0.0376 0.1243 0.1262]		
R08	[-0.0473 -0.0335 0.1650 0.1682]	[-0.1462 0.0675 0.0969 0.1016]		
R09	[-0.1724 0.1287 0.1925 0.1981]	[-0.3212 -0.0996 -0.0333 0.1230]		
R10	[-0.2025 -0.1748 -0.0634 0.1793]	[-0.3553 -0.3542 -0.2916 -0.2281]		
R11	[-0.1725 -0.1621 -0.0334 0.1470]	[0.0129 0.0402 0.1089 0.1098]		
R12	[-0.1974 -0.0545 0.0367 0.1453]	[-0.2792 -0.2465 -0.2343 -0.1967]		

Appendix B. The Welding plan of the validation

This table is containing the welding plan used in the validation test.

Table B.1
Welding Plan of the Validation test workpiece.

ID	*TCP.X*	*TCP.Y*	*TCP.A*	*U*	*I*	v_t	v_f	*BC.X*	*BC.Y*	$B.a_0$	$B.a_1$	$B.a_2$
0	-0.3	7.47	0	12	200	3	750	-0.30	4.37	5.4920	0.0654	0.0918
1	-0.2	9.55	0	12	200	3	850	-0.30	5.52	6.8347	-0.0023	0.0217
2	-0.3	10.97	0	12	200	2.8	850	-0.30	6.85	7.7877	-0.0866	0.0268
3	-1.5	12.15	-3	12	200	2.7	900	-1.71	8.12	8.8517	-0.2557	-0.0057
4	1.5	13.17	3	12	200	2.7	900	1.75	8.44	9.3281	0.0258	0.0223
5	-1.9	13.53	-4	12	200	2.7	940	-2.19	9.36	10.2024	-0.1822	0.0064
6	1.9	14.01	4	12	200	2.6	940	2.19	9.86	10.8621	0.1095	-0.0126
7	-2.4	14.68	-4	12	200	2.6	1000	-2.67	10.75	11.7516	-0.1608	-0.0104
8	2.3	15.15	4	12	200	2.5	1000	2.57	11.29	12.4366	0.1912	-0.0510
9	-3.4	15.79	-4	12	200	2.5	1000	-3.65	12.18	13.0106	-0.1557	-0.0101
10	4.8	16.56	4	12	200	2.5	1000	5.11	12.08	13.0130	0.0273	0.0123
11	-4.5	16.91	-4	12	220	2.5	1250	-4.73	13.59	13.6945	-0.3465	-0.0160
12	5.5	17.17	4	12	220	2.5	1250	5.75	13.64	13.5775	0.3179	-0.0137
13	-0.3	17.65	0	12	220	2.5	1250	-0.30	13.85	15.5010	-0.0042	-0.0230
14	-5.6	18.44	-4	12	220	2.5	1350	-5.83	15.08	15.5598	-0.2796	-0.0097
15	6.4	18.35	4	12	220	2.4	1350	6.63	15.05	15.2733	0.2637	-0.0092
16	-0.3	18.76	0	12	220	2.4	1350	-0.30	15.71	17.3456	-0.0213	-0.0289
17	-6.5	20.14	-4	12	220	2.4	1400	-6.72	16.97	17.2876	-0.3165	-0.0169
18	7.4	19.99	4	12	220	2.3	1400	7.63	16.76	16.7304	0.3269	-0.0148
19	-0.3	20.71	0	12	220	2.3	1400	-0.30	17.33	19.1085	-0.0328	-0.0281
20	-8	21.99	-4	12	220	2.3	1450	-8.23	18.73	18.5027	-0.3571	-0.0151
21	8.4	21.52	4	12	220	2.25	1450	8.62	18.37	17.8342	0.4462	-0.0237
22	-0.3	22.18	0	12	220	2.25	1450	-0.30	19.04	20.6201	-0.0258	-0.0277
23	-9	23.29	4	12	230	2.25	1580	-8.80	20.43	19.6807	-0.3634	-0.0109
24	9.4	22.62	-4	12	230	2.3	1580	9.21	19.92	19.3076	0.3614	-0.0141
25	-0.3	23.62	0	12	230	2.3	1580	-0.30	20.62	22.1004	-0.0233	-0.0313
26	-10	24.96	-4	12	240	2.3	1750	-10.19	22.22	19.9808	-0.6580	-0.0270
27	10.4	24.58	4	12	240	2.3	1750	10.62	21.50	19.9740	0.4347	-0.0125
28	-0.3	24.69	0	12	240	2.3	1750	-0.30	22.12	23.6100	-0.0556	-0.0380
29	-9	25.88	-4	12	240	2.3	1700	-9.15	23.73	22.1127	-0.6774	-0.0392
30	9.4	25.48	4	12	240	2.3	1700	9.58	22.95	20.8302	0.7712	-0.0402

References

Alfaro, S. C. A., & Franco, F. D. (2010). Exploring Infrared Sensoring for Real Time Welding Defects Monitoring in GTAW. *Sensors, 10*(6), 5962–5974. https://doi.org/10.3390/s100605962. http://www.mdpi.com/1424-8220/10/6/5962.

American Welding Society, A., Jan. 2001. Welding Handbook: Welding Science and Technology, 9th Edition. Vol. 1. American Welding Society, Miami, FL.

Balázs, K., Botzheim, J., & Kóczy, L. T. (2010). Comparative Investigation of Various Evolutionary and Memetic Algorithms. In *Computational Intelligence in Engineering. Vol. 313 of Studies in Computational Intelligence* (pp. 129–140). Berlin Heidelberg, Berlin, Heidelberg: Springer. https://doi.org/10.1007/978-3-642-15220-7.

Balázs, K., Botzheim, J., & Kóczy, L. T. (2010). Comparative Investigation of Various Evolutionary and Memetic Algorithms. In J. Kacprzyk, I. J. Rudas, J. Fodor, & J. Kacprzyk (Eds.), *series Title: Studies in Computational Intelligence: Vol. 313. Computational Intelligence in Engineering* (pp. 129–140). Berlin Heidelberg, Berlin, Heidelberg: Springer. https://doi.org/10.1007/978-3-642-15220-7_11.

Bartz-Beielstein, T., Branke, J., Mehnen, J., & Mersmann, O. (2014). Evolutionary Algorithms. Wiley Interdisciplinary Reviews. *Data Mining and Knowledge Discovery, 4*(3), 178–195. https://doi.org/10.1002/widm.1124

Benyounis, K. Y., & Olabi, A. G. (2008). Optimization of different welding processes using statistical and numerical approaches – A reference guide. *Advances in Engineering Software, 39*(6), 483–496. https://doi.org/10.1016/j.advengsoft.2007.03.012. URL: http://www.sciencedirect.com/science/article/pii/S0965997807001020.

Botzheim, J., Cabrita, C., Koczy, L., Ruano, A., 2004. Estimating fuzzy membership functions parameters by the Levenberg-Marquardt algorithm. In: 2004 IEEE International Conference on Fuzzy Systems (IEEE Cat. No.04CH37542). Vol. 3. pp. 1667–1672 vol 3, iSSN: 1098–7584. doi: 10.1109/FUZZY.2004.1375431.

Botzheim, J., Cabrita, C., Kóczy, L. T., & Ruano, A. E. (2009). Fuzzy rule extraction by bacterial memetic algorithms. *International Journal of Intelligent Systems, 24*(3), 312–339. https://doi.org/10.1002/int.20338. URL: https://onlinelibrary.wiley.com/doi/abs/10.1002/int.20338.

Botzheim, J., & Földesi, P. (2014). Novel calculation of fuzzy exponent in the sigmoid functions for fuzzy neural networks. *Neurocomputing, 129*, 458–466. https://doi.org/10.1016/j.neucom.2013.09.013. URL: http://www.sciencedirect.com/science/article/pii/S0925231213009211.

Botzheim, J., Toda, Y., & Kubota, N. (2012). Bacterial memetic algorithm for offline path planning of mobile robots. *Memetic Computing, 4*(1), 73–86. https://doi.org/10.1007/s12293-012-0076-0. URL: http://link.springer.com/10.1007/s12293-012-0076-0.

Bódis, T., & Botzheim, J. (2018). Bacterial Memetic Algorithms for Order Picking Routing Problem with Loading Constraints. *Expert Systems with Applications, 105*, 196–220. https://doi.org/10.1016/j.eswa.2018.03.043. URL: http://www.sciencedirect.com/science/article/pii/S0957417418301891.

Cao, Y., Zhu, S., Liang, X., & Wang, W. (2011). Overlapping model of beads and curve fitting of bead section for rapid manufacturing by robotic MAG welding process. *Robotics and Computer-Integrated Manufacturing, 27*(3), 641–645. https://doi.org/10.1016/j.rcim.2010.11.002. URL: https://www.sciencedirect.com/science/article/pii/S0736584510001729.

Cordón, O. (Ed.), 2001. Genetic fuzzy systems: evolutionary tuning and learning of fuzzy knowledge bases. No. v. 19 in Advances in fuzzy systems. World Scientific, Singapore, oCLC: ocm47768307.

DebRoy, T., Wei, H., Zuback, J., Mukherjee, T., Elmer, J., Milewski, J., Beese, A., Wilson-Heid, A., De, A., & Zhang, W. (2018). Additive manufacturing of metallic components – Process, structure and properties. *Progress in Materials Science, 92*, 112–224. https://doi.org/10.1016/j.pmatsci.2017.10.001. URL: https://linkinghub.elsevier.com/retrieve/pii/S0079642517301172.

Ding, D., Pan, Z., Cuiuri, D., & Li, H. (2015). A multi-bead overlapping model for robotic wire and arc additive manufacturing (WAAM). *Robotics and Computer-Integrated Manufacturing, 31*, 101–110. https://doi.org/10.1016/j.rcim.2014.08.008. URL: http://www.sciencedirect.com/science/article/pii/S0736584514000696.

Ding, D., Shen, C., Pan, Z., Cuiuri, D., Li, H., Larkin, N., & van Duin, S. (2016). Towards an automated robotic arc-welding-based additive manufacturing system from CAD to finished part. *Computer-Aided Design, 73*, 66–75. https://doi.org/10.1016/j.cad.2015.12.003. URL: http://linkinghub.elsevier.com/retrieve/pii/S0010448515001748.

Doerr, B., Neumann, F. (Eds.), 2020. Theory of Evolutionary Computation: Recent Developments in Discrete Optimization. Natural Computing Series. Springer International Publishing, Cham. URL http://link.springer.com/10.1007/978-3-030-29414-4 doi: 10.1007/978-3-030-29414-4.

Dutta, P., & Pratihar, D. K. (2007). Modeling of TIG welding process using conventional regression analysis and neural network-based approaches. *Journal of Materials Processing Technology, 184*(1–3), 56–68. https://doi.org/10.1016/j.jmatprotec.2006.11.004. URL: http://www.sciencedirect.com/science/article/pii/S0924013606009137.

Fan, D., Zhang, G., Shi, Y., & Zhu, M. (2019). Progress and Trend in Intelligent Sensing and Control of Weld Pool in Arc Welding Process. In S. Chen, Y. Zhang, & Z. Feng (Eds.), *Transactions on Intelligent Welding Manufacturing. Transactions on Intelligent Welding Manufacturing* (pp. 27–43). Singapore: Springer. https://doi.org/10.1007/978-981-13-7418-0.

Fang, H. C., Ong, S. K., & Nee, A. Y. C. (2012). Interactive robot trajectory planning and simulation using Augmented Reality. *Robotics and Computer-Integrated Manufacturing, 28*(2), 227–237. https://doi.org/10.1016/j.rcim.2011.09.003. URL: http://www.sciencedirect.com/science/article/pii/S0736584511001116.

Fang, H. C., Ong, S. K., & Nee, A. Y. C. (2016). Robot path planning optimization for welding complex joints. *The International Journal of Advanced Manufacturing Technology*, 1–11. https://doi.org/10.1007/s00170-016-9684-z. URL: https://link.springer.com/article/10.1007/s00170-016-9684-z.

Fang, H. C., Ong, S. K., & Nee, A. Y. C. (2017). Adaptive pass planning and optimization for robotic welding of complex joints. *Advances in Manufacturing, 5*(2), 93–104. https://doi.org/10.1007/s40436-017-0181-x. URL: http://link.springer.com/10.1007/s40436-017-0181-x.

Feng, Y., Chen, Z., Wang, D., Chen, J., & Feng, Z. (Jan. 2020). DeepWelding: A Deep Learning Enhanced Approach to GTAW Using Multisource Sensing Images. *IEEE Transactions on Industrial Informatics, 16*(1), 465–474. https://doi.org/10.1109/TII.2019.2937563

Fernandez, A., Herrera, F., Cordon, O., Jose del Jesus, M., Marcelloni, F., Feb. 2019. Evolutionary Fuzzy Systems for Explainable Artificial Intelligence: Why, When, What for, and Where to? IEEE Computational Intelligence Magazine 14 (1), 69–81, conference Name: IEEE Computational Intelligence Magazine. doi: 10.1109/MCI.2018.2881645.

Gowtham, K. N., Vasudevan, M., Maduraimuthu, V., & Jayakumar, T. (2011). Intelligent Modeling Combining Adaptive Neuro Fuzzy Inference System and Genetic Algorithm for Optimizing Welding Process Parameters. *Metallurgical and Materials Transactions B, 42*(2), 385–392. https://doi.org/10.1007/s11663-010-9471-4

Hancheng, Q., Bocai, X., Shangzheng, L., & Fagen, W. (2002). Fuzzy neural network modeling of material properties. *Journal of Materials Processing Technology, 122*(2), 196–200. https://doi.org/10.1016/S0924-0136(02)00019-5. URL: http://www.sciencedirect.com/science/article/pii/S0924013602000195.

Horvath, C. M., Thomessen, T., Korondi, P., Jun. 2017. Robotized Multi-Pass Tungsten Inner Gas Welding of Francis Hydro Power Turbines. In: 2017 IEEE International Symposium on Industrial Electronics. IEEE IES, Edinburgh, Scotland, United Kingdom, pp. 1759–1765. URL https://ieeexplore.ieee.org/document/8001514 doi: 10.1109/ISIE.2017.8001514.

Horváth, C. M., Botzheim, J., Thomessen, T., Korondi, P., 2020. Bacterial Memetic Algorithm Trained Fuzzy System-Based Model of Single Weld Bead Geometry. IEEE Access 8, 164864–164881, iF:3.745. URL https://ieeexplore.ieee.org/document/9186598 doi: 10.1109/ACCESS.2020.3021950.

Horváth, C. M., & Korondi, P. (2018). Supportive Robotic Welding System for Heavy, Small Series Production with Non-Uniform Welding Grooves. *Acta Polytechnica Hungarica, 15*(8), 141–165. https://doi.org/10.12700/APH.15.8.2018.8.7

Jang, J.-S., & Sun, C.-T. (1993). Functional equivalence between radial basis function networks and fuzzy inference systems. *IEEE Transactions on Neural Networks, 4*(1), 156–159. https://doi.org/10.1109/72.182710. URL: http://ieeexplore.ieee.org/document/182710/.

Joshi, S., Hildebrand, J., Aloraier, A. S., & Rabczuk, T. (2013). Characterization of material properties and heat source parameters in welding simulation of two overlapping beads on a substrate plate. *Computational Materials Science, 69*, 559–565. https://doi.org/10.1016/j.commatsci.2012.11.029. URL: http://www.sciencedirect.com/science/article/pii/S092702561200688X.

Kacker, R. N., Lagergren, E. S., & Filliben, J. J. (1991). Taguchi's Orthogonal Arrays Are Classical Designs of Experiments. *Journal of Research of the National Institute of Standards and Technology, 96*(5), 577–591. https://doi.org/10.6028/jres.096.034. URL: https://www.ncbi.nlm.nih.gov/pmc/articles/PMC4927234/.

Kesse, M. A., Buah, E., Handroos, H., Ayetor, G. K., Apr. 2020. Development of an Artificial Intelligence Powered TIG Welding Algorithm for the Prediction of Bead Geometry for TIG Welding Processes using Hybrid Deep Learning. Metals 10 (4), 451, number: 4 Publisher: Multidisciplinary Digital Publishing Institute. https://www.mdpi.com/2075-4701/10/4/451 doi: 10.3390/met10040451.

Kim, I. S., Son, J. S., Park, C. E., Lee, C. W., & Prasad, Y. K. D. V. (2002). A study on prediction of bead height in robotic arc welding using a neural network. *Journal of Materials Processing Technology, 130–131*, 229–234. https://doi.org/10.1016/S0924-0136(02)00803-8. URL: http://www.sciencedirect.com/science/article/pii/S0924013602008038.

Koczy, L. (1996). Fuzzy if...then rule models and their transformation into one another. *IEEE Transactions on Systems, Man, and Cybernetics - Part A: Systems and Humans, 26*(5), 621–637. https://doi.org/10.1109/3468.531909

Koczy, L. T., Tikk, D., & Gedeon, T. D. (2000). On functional equivalence of certain fuzzy controllers and RBF type approximation schemes. *International Journal of Fuzzy Systems, 2*(3), 164–175.

Kurková, V. (1992). Kolmogorov's theorem and multilayer neural networks. *Neural Networks, 5*(3), 501–506. https://doi.org/10.1016/0893-6080(92)90012-8. URL: http://www.sciencedirect.com/science/article/pii/0893608092900128.

Lee, D., Ku, N., Kim, T.-W., Kim, J., Lee, K.-Y., & Son, Y.-S. (2011). Development and application of an intelligent welding robot system for shipbuilding. *Robotics and Computer-Integrated Manufacturing, 27*(2), 377–388. https://doi.org/10.1016/j.rcim.2010.08.006. URL: http://www.sciencedirect.com/science/article/pii/S0736584510001055.

Levenberg, K., 1944. A method for the solution of certain non-linear problems in least squares. Quarterly of Applied Mathematics 2 (2), 164–168, publisher: Brown University. https://www.jstor.org/stable/43633451.

Li, Y., Sun, Y., Han, Q., Zhang, G., & Horváth, I. (2018). Enhanced beads overlapping model for wire and arc additive manufacturing of multi-layer multi-bead metallic parts. *Journal of Materials Processing Technology, 252*, 838–848. https://doi.org/10.1016/j.jmatprotec.2017.10.017. URL: http://linkinghub.elsevier.com/retrieve/pii/S0924013617304661.

Liao, T. W. (2003). Classification of welding flaw types with fuzzy expert systems. *Expert Systems with Applications, 25*(1), 101–111. https://doi.org/10.1016/S0957-4174(03)00010-1. URL: http://www.sciencedirect.com/science/article/pii/S0957417403000101.

Liu, Y., Zhang, W., & Zhang, Y. (2015). Dynamic Neuro-Fuzzy-Based Human Intelligence Modeling and Control in GTAW. *IEEE Transactions on Automation Science and Engineering, 12*(1), 324–335. https://doi.org/10.1109/TASE.2013.2279157. URL: https://ieeexplore.ieee.org/document/6589144.

Liu, Y., & Zhang, Y. (2015). Iterative Local ANFIS-Based Human Welder Intelligence Modeling and Control in Pipe GTAW Process: A Data-Driven Approach. *IEEE/ASME Transactions on Mechatronics, 20*(3), 1079–1088. https://doi.org/10.1109/TMECH.2014.2363050. URL: https://ieeexplore.ieee.org/document/6949113.

Madsen, O., Bro Soerensen, C., Larsen, R., Overgaard, L., Jacobsen, N. J., Apr. 2002. A system for complex robotic welding. Industrial Robot: An International Journal 29 (2), 127–131, read. http://www.emeraldinsight.com/doi/abs/10.1108/01439910210419132 doi: 10.1108/01439910210419132.

Mamdani, E. H., & Assilian, S. (1975). An experiment in linguistic synthesis with a fuzzy logic controller. *International Journal of Man-Machine Studies, 7*(1), 1–13. https://doi.org/10.1016/S0020-7373(75)80002-2. URL: http://www.sciencedirect.com/science/article/pii/S0020737375800022.

Marquardt, D. W. (1963). An algorithm for least-squares estimation of nonlinear parameters. *Journal of the society for Industrial and Applied Mathematics, 11*(2), 431–441.

Meng, X., Qin, G., & Zou, Z. (2017). Sensitivity of driving forces on molten pool behavior and defect formation in high-speed gas tungsten arc welding. *International Journal of Heat and Mass Transfer, 107*, 1119–1128. https://doi.org/10.1016/j.ijheatmasstransfer.2016.11.025. URL: http://www.sciencedirect.com/science/article/pii/S0017931016319639.

Mishra, S., & DebRoy, T. (2007). Tailoring gas tungsten arc weld geometry using a genetic algorithm and a neural network trained with convective heat flow calculations. *Materials Science and Engineering: A, 454–455*, 477–486. https://doi.org/10.1016/j.msea.2006.11.149. URL: http://www.sciencedirect.com/science/article/pii/S0921509306025111.

Moscato, P., 1989. On Evolution, Search, Optimization, Genetic Algorithms and Martial Arts - Towards Memetic Algorithms. Tech. Rep. C3P Report 826, California Institute of Technology, Pasadena, California, doi: 10.1.1.27.9474. http://citeseerx.ist.psu.edu/viewdoc/summary?doi=10.1.1.27.9474.

Narang, H. K., Singh, U. P., Mahapatra, M. M., Jha, P. K., 2011. Prediction of the weld pool geometry of TIG arc welding by using fuzzy logic controller. International Journal of Engineering, Science and Technology 3 (9), 77–85, number: 9. https://www.ajol.info/index.php/ijest/article/view/82198 doi: 10.4314/ijest.v3i9.6.

Nawa, N., & Furuhashi, T. (Oct. 1999). Fuzzy system parameters discovery by bacterial evolutionary algorithm. *IEEE Transactions on Fuzzy Systems, 7*(5), 608–616. https://doi.org/10.1109/91.797983

Palani, P. K., & Murugan, N. (2007). Optimization of weld bead geometry for stainless steel claddings deposited by FCAW. *Journal of Materials Processing Technology, 190*(1–3), 291–299. https://doi.org/10.1016/j.jmatprotec.2007.02.035. URL: http://www.sciencedirect.com/science/article/pii/S0924013607001732.

Pires, J. N., Loureiro, A., & Bolmsjö, G. (2006). *Welding Robots: Technology, System Issues and Application*. Springer Science & Business Media. https://doi.org/10.1007/1-84628-191-1

Pratihar, D. K. (2015). Expert systems in manufacturing processes using soft computing. *International Journal of Advanced Manufacturing Technology, 1–10*. https://doi.org/10.1007/s00170-015-7285-x

Schneider, C. F., Lisboa, C. P., Silva, R. d. A., Lermen, R. T., Oct. 2017. Optimizing the Parameters of TIG-MIG/MAG Hybrid Welding on the Geometry of Bead Welding Using the Taguchi Method. Journal of Manufacturing and Materials Processing 1 (2), 14. URL http://www.mdpi.com/2504-4494/1/2/14 doi: 10.3390/jmmp1020014.

Somlo, K., & Sziebig, G. (2019). Aspects of Multi-pass GTAW of Low Alloyed Steels. *IFAC-PapersOnLine, 52*(22), 101–107. https://doi.org/10.1016/j.ifacol.2019.11.056. URL: http://www.sciencedirect.com/science/article/pii/S2405896319309917.

Subashini, L., & Vasudevan, M. (2012). Adaptive Neuro-Fuzzy Inference System (ANFIS)-Based Models for Predicting the Weld Bead Width and Depth of Penetration from the Infrared Thermal Image of the Weld Pool. *Metallurgical and Materials Transactions B, 43*(1), 145–154. https://doi.org/10.1007/s11663-011-9570-x

Suryakumar, S., Karunakaran, K. P., Bernard, A., Chandrasekhar, U., Raghavender, N., Sharma, D., Apr. 2011. Weld bead modeling and process optimization in Hybrid Layered Manufacturing. Computer-Aided Design 43 (4), 331–344. URL https://www.sciencedirect.com/science/article/pii/S0010448511000078 doi: 10.1016/j.cad.2011.01.006.

Tarn, T.-J., Chen, S.-B., Fang, G. (Eds.), 2011. Robotic Welding, Intelligence and Automation. Vol. 88 of Lecture Notes in Electrical Engineering. Springer, Berlin Heidelberg, Berlin, Heidelberg. http://link.springer.com/10.1007/978-3-642-19959-2.

Wang, L.-X. (1992). Fuzzy systems are universal approximators. In *[1992 Proceedings] IEEE International Conference on Fuzzy Systems* (pp. 1163–1170). https://doi.org/10.1109/FUZZY.1992.258721

Wang, Y., Zhang, C., Lu, J., Bai, L., Zhao, Z., & Han, J. (2020). Weld Reinforcement Analysis Based on Long-Term Prediction of Molten Pool Image in Additive Manufacturing. *IEEE Access, 8*, 69908–69918. https://doi.org/10.1109/ACCESS.2020.2986130

Wu, Y., Go, J. Z. M., Ahmed, S. M., Lu, W.-F., Chew, C.-M., & Pang, C. K. (2015). Automated bead layout methodology for robotic multi-pass welding. In *2015 IEEE 20th Conference on Emerging Technologies & Factory Automation (ETFA)* (pp. 1–4). Luxemburg: IEEE.

Xiong, J., Zhang, G., Gao, H., & Wu, L. (2013). Modeling of bead section profile and overlapping beads with experimental validation for robotic GMAW-based rapid manufacturing. *Robotics and Computer-Integrated Manufacturing, 29*(2), 417–423. https://doi.org/10.1016/j.rcim.2012.09.011. URL: https://www.sciencedirect.com/science/article/pii/S0736584512001147.

Xiong, J., Zhang, G., Hu, J., & Wu, L. (2014). Bead geometry prediction for robotic GMAW-based rapid manufacturing through a neural network and a second-order regression analysis. *Journal of Intelligent Manufacturing, 25*(1), 157–163. https://doi.org/10.1007/s10845-012-0682-1. URL: https://link.springer.com/article/10.1007/s10845-012-0682-1.

Xue, Y., Kim, I. S., Son, J. S., Park, C. E., Kim, H. H., Sung, B. S., Kim, I. J., Kim, H. J., & Kang, B. Y. (2005). Fuzzy regression method for prediction and control the bead width in the robotic arc-welding process. *Journal of Materials Processing Technology, 164–165*, 1134–1139. https://doi.org/10.1016/j.jmatprotec.2005.02.174. URL: http://www.sciencedirect.com/science/article/pii/S0924013605002220.

Yan, S., Fang, H., Ong, S., & Nee, A. (2017). Optimal pass planning for robotic welding of large-dimension joints with nonuniform grooves. *Proceedings of the Institution of Mechanical Engineers, Part B: Journal of Engineering Manufacture*. https://doi.org/10.1177/0954405417718877

Yan, S., Ong, S., & Nee, A. (2016). Optimal Pass Planning for Robotic Welding of Large-dimension Joints with Deep Grooves. *Procedia CIRP, 56*, 188–192. https://doi.org/10.1016/j.procir.2016.10.052. URL: http://linkinghub.elsevier.com/retrieve/pii/S2212827116310447.

Yang, C., Ye, Z., Chen, Y., Zhong, J., & Chen, S. (2014). Multi-pass path planning for thick plate by DSAW based on vision sensor. *Sensor Review, 34*(4), 416–423. https://doi.org/10.1108/SR-04-2013-649. URL: http://www.emeraldinsight.com/doi/full/10.1108/SR-04-2013-649.

Yuan, L., Ding, D., Pan, Z., Yu, Z., Wu, B., van Duin, S., Li, H., & Li, W. (2020). Application of Multidirectional Robotic Wire Arc Additive Manufacturing Process for the Fabrication of Complex Metallic Parts. *IEEE Transactions on Industrial Informatics, 16*(1), 454–464. https://doi.org/10.1109/TII.2019.2935233

Zhang, H., Lu, H., Cai, C., Chen, S., 2011. Robot Path Planning in Multi-pass Weaving Welding for Thick Plates. In: Tarn, T.-J., Chen, S.-B., Fang, G. (Eds.), Robotic Welding, Intelligence and Automation. No. 88 in Lecture Notes in Electrical Engineering. Springer, Berlin Heidelberg, pp. 351–359. http://link.springer.com/chapter/10.1007/978-3-642-19959-2-43 doi: 10.1007/978-3-642-19959-2-43.

Zhou, D., Fang, Y., Botzheim, J., Kubota, N., & Liu, H. (2016). Bacterial memetic algorithm based feature selection for surface EMG based hand motion recognition in long-term use. In *2016 IEEE Symposium Series on Computational Intelligence (SSCI)* (pp. 1–7). https://doi.org/10.1109/SSCI.2016.7850241